Bioconjugate Chemistry

Article

Hypoxia-activated and indomethacin-mediated theranostic prodrug releasing drug on-demand for tumor imaging and therapy

Xiaoran Peng, Jiaxin Gao, Yumeng Yuan, Haitong Liu,
Weiyan Lei, Shenghui Li, Jinchao Zhang, and Shuxiang Wang

Bioconjugate Chem., **Just Accepted Manuscript** • DOI: 10.1021/acs.bioconjchem.9b00564 • Publication Date (Web): 08 Oct 2019

Just Accepted

is published by the American Chemical Society. 1155 Sixteenth Street N.W., Washington, DC 20036

Graphical abstract

Hypoxia-activated and indomethacin-mediated theranostic prodrug releasing drug on-demand for tumor imaging and therapy

Xiaoran Peng, Jiaxin Gao, Yumeng Yuan, Haitong Liu, Weiyan Lei, Shenghui Li, Jinchao Zhang, and Shuxiang Wang

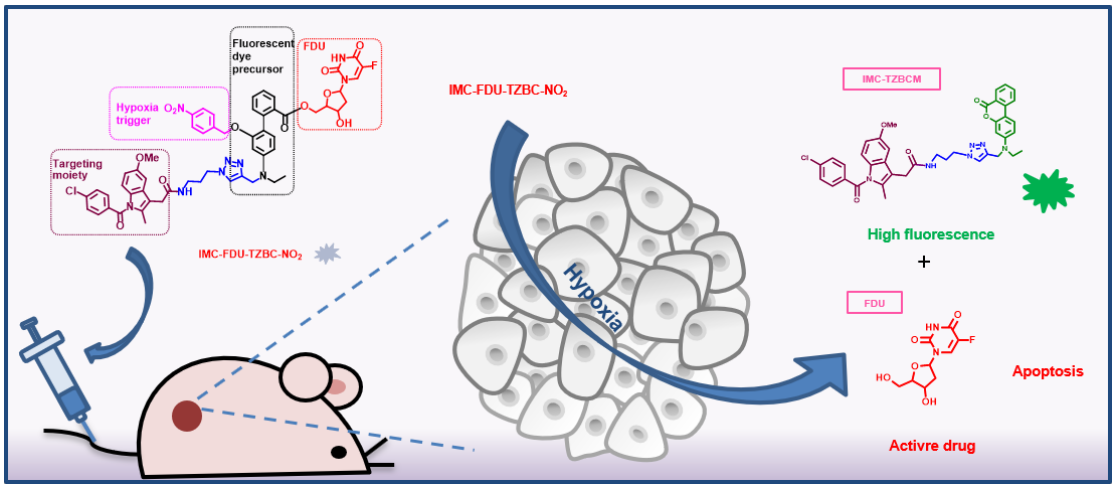

Hypoxia-Activated and Indomethacin-Mediated Theranostic Prodrug Releasing Drug on-Demand for Tumor Imaging and Therapy

Xiaoran Peng,[a] Jiaxin Gao,[a] Yumeng Yuan,[a] Haitong Liu,[a] Weiyan Lei,[a] Shenghui Li,[a,b] Jinchao Zhang, *[a,b] and Shuxiang Wang*[a,b]

[a]*Key Laboratory of Medicinal Chemistry and Molecular Diagnosis of Ministry of Education, Hebei University, Baoding 071002, China*

[b]*Key Laboratory of Chemical Biology of Hebei Province, College of Chemistry and Environmental Science, Hebei University, Baoding 071002, China*

Email: jczhang6970@163.com; wsx@hbu.edu.cn

Supporting Information

ABSTRACT: A smart theranostic prodrug IMC-FDU-TZBC-NO_2, releasing active drug on-demand based on hypoxia-activated and indomethacin-mediated, for solid tumor imaging and efficient therapy was designed. This prodrug was constructed by conjugating of chemotherapy drug 5-fluoro-2-deoxyuridine (FDU), targeting moiety indomethacin (IMC), and hypoxic trigger 4-nitrobenzyl group to a fluorescent dye precursor, which was mediated by IMC and activated by NTR under hypoxia conditions. The fluorescent dye IMC-TZBCM was generated and FDU was released at the same time in tumor cells. The rates and amounts of FDU release and IMC-TZBCM generation were regulated by hypoxia status, and increased with increasing degree of hypoxia. Nevertheless, it is "locked" in normal cells. It combined the advantages of tumor targeting, diagnosis, and chemotherapy functions together, showed excellent targeting ability to cancer cells, excellent stability in physiological conditions, high cellular uptake efficiency, and on-demand drug release behavior. The *in vitro* and *in vivo* assays demonstrated that IMC-FDU-TZBC-NO_2 exhibiting enhanced anticancer potency and low side effect. The novel targeted theranostic prodrug activated by hypoxia shows a great potential in cancer therapy.

■ INTRODUCTION

In recent years, the incidence of cancer and death rates have continued to rise,[1] and chemotherapy is a main stream approach for cancer therapy.[2] Despite several anticancer drugs such as doxorubicin (DOX), paclitaxel, camptothecin (CPT), fluorouracil, and gemcitabine were approved by the FDA, it is a formidable challenge to achieve the desired therapeutic effect with minimum side effects, since these chemotherapy strategies are based on high doses and poor selectivity for tumor cells, which results in side effects and drug resistance.[3] Therefore, considerable efforts have been devoted to explore efficient strategies of prodrugs, aiming at improving anticancer drugs specifically into tumors and on-demand releasing with controlled temporal profile to enhance therapeutic efficacy and reduce side effects.[4] In particular, theranostic agents with both therapeutic and diagnostic functions are attracting great interest due to their reduced side effects, and enhanced clinical efficacy.[5-8] Theses theranostic agents were triggered by specific internal or external stimulus (such as high acidity,[9-14] over-expressed

enzymes,[15-22] reactive oxygen species,[23-28] heat,[29, 30] and light,[31-33] etc.), and have been developed for releasing drugs on demand inside the tumor and real-time tracking of drug release and localization. Among these stimulation ways, over-expressed enzymes-responsive theranostic agents have drawn great attention because of this strategy seeks to treat cancer through the selective identification and therapeutics in cancer tissue.

Hypoxia as a common feature of all solid tumors is associated with the tumor growth,[34, 35] angiogenesis,[36] invasion,[37] angiogenesis, recurrence, and metastatsis.[38] Therefore, hypoxia is an indicator of poor prognosis and therapeutic outcome, resistance to chemotherapy, and recurrence.[39] However, hypoxia also provides a hopefully useable target for cancer diagnosis and treatment. In hypoxic solid tumors, nitroreductase (NTR) is over-expressed, which can be used as trigger for design selective anticancer prodrug. Therefore, hypoxia activation provides a pathway for hypoxia-activated prodrug to release drug on-demand. A number of prodrugs activated by NTR under hypoxia conditions have been developed to improve tumor-selective chemotherapeutic effects.[40-43] TH-302 as a hypoxia-activated prodrug showed promise therapeutic effect in preclinical and phase II trials.[44] However, it was reported that TH-302 did not achieve primary overall survival endpoints in combination with chemotherapy in two large phase III studies.[45] Thus, targeting and controllable release of active drug at tumor sites is a challenge for tumor therapy.

Cyclooxygenase (COX) is a key enzyme that plays a decisive role in catalyzing transformation of arachidonic acid to prostaglandins, which in turn contributes to inflammation and tumorigenesis in humans.[46] Indeed, COX-2 over-expression and antiproliferative effects of COX-2 inhibitors have been reported in various cancers (such as pancreatic, colon cancer, liver, and gastric cancers).[47-50] And, COX-2 critically influences all stages of tumor progression from initiation to progression. Therefore COX-2 can be used as an ideal target for tumor diagnosis and treatment.[51-53] As an inhibitor of COX-2, indomethacin (IMC) exhibited a great potential in the identification and quantification of COX-2 in biological systems[54] and has been used to distinguish between normal, inflammatory, and cancer cells.[52]

In this work, we developed a novel theranostic prodrug, IMC-FDU-TZBC-NO_2, based on hypoxia-activation and IMC-guiding for on-demand drug release and enhanced anticancer potency with low side effect. In this design (Scheme 1)， 5-fluoro-2-deoxyuridine (FDU) was chosen as the active drug due to displaying high antitumor activity, hydrophilicity, [55, 56] and being widely used in the treatments of cancer. IMC was used as a targeting moiety to improve the drug targeting effect,[57] cellular uptake efficiency, and drug accumulation; 4-nitrobenzyl group was used as a trigger to hypoxia to release active drug on demand based on hypoxic status; 1,1'-biphenyl-4'-((1H-1,2,3-triazol-4-yl)methyl)ethylamino-2'-(4-nitrobenzyloxy)-2-carboxylate (BPBC-NO_2) was used as a fluorescent dye precursor for formation a fluorescent dye IMC-TZBCM under hypoxia conditions; and BPBC-NO_2 was connected with IMC, 4-nitrobenzyl group, and FDU by covalent bonds. The obtained IMC-FDU-TZBC-NO_2 not only can target tumor cells, but also are able to release IMC-TZBCM and FDU simultaneously under hypoxic conditions for investigating the hypoxic status, *in vitro* and *in vivo* inhibition of tumor cell growth with high efficiency and minimal side effects. This strategy will provide a valuable tool for cancer therapy on individual patient's demand based on the individual hypoxic status.

Scheme 1. Structure and Schematic Illustration of IMC-FDU-TZBC-NO_2

Scheme 1

■ RESULTS AND DSISCUSSION

Synthesis and Characterization. To examine the effectiveness of this strategy, IMC-TZBCM, FDU-TZBC-NO_2, and IMC-mediated theranostic prodrug IMC-FDU-TZBC-NO_2 were synthesized (Scheme 2). Firstly, the ethylation reaction of 4-bromo-3-methoxyaniline with bromoethane in dry DMF afforded compound **1**. Subsequently, the demethylation of compound **1** by BBr_3 afforded compound **2**. Then, compound **2** was protected at the arylamine *N* by means of $(Boc)_2O$ to afford compound **3** at room temperature. Followed by nucleophilic substitution of compound 3 with 4-nitrobenzyl-bromide, *t*-butyl (4-bromo-3-((4-nitrobenzyl)oxy)phenyl) ethylcarbamate (**4**) was generated. Subsequently, ethyl 4'-((*t*-butoxycarbonyl)ethylamino)-2'-((4-nitrobenzyl)oxy)-1,1'-biphenyl-2-carboxylate (**5**) was synthesized *via* Suzuki cross-couping reaction between compound **4** with 2-(ethoxycarbonyl)phenyl boronic acid under N_2 atmosphere. Next, *N*-boc deprotection of compound **5** was achieved by a solution of HCl (4 M) in anhydrous THF to afford ethyl 4'-(ethylamino)-2'-((4-nitrobenzyl)oxy)-1,1'-biphenyl-2-carboxylate (**6**). Followed by nucleophilic substitution of compound **6** with 3-bromoprop-1-yne, ethyl 4'-(ethyl(prop-2-yn-1-yl)amino)-2'-((4-nitrobenzyl)oxy)-1,1'-biphenyl-2-carboxylate (**7**) was generated. Afterwards, take advantage of hydrolysis of compound **7** in sulfuric acid aqueous solution, 4'-(ethyl(prop-2-yn-1-yl)amino)-2'-((4-nitrobenzyl)oxy)-1,1'-biphenyl-2-carboxylic acid (**8**) was obtained. Then, FDU was conjugated with compound **8** to provide FDU-TZBC-NO_2 (as the control drug) using DIC as condensation agent and catalytic amount of DMAP. Meanwhile, IMC was modified by azidopropan-1-amine *via* an amidation reaction in presence of HATU to afford IMC-N_3. Then, IMC-TZBC-NO_2 was generated by the click reaction of IMC-N_3 with compound **8** at 25 °C in the presence of Vc and $CuSO_4$. Finally, IMC-FDU-TZBC-NO_2 was constructed *via* an amidation reaction of FDU with IMC-TZBC-NO_2 in the presence of DIC and DMAP. And, in the presence of $Na_2S_2O_4$, IMC-TZBC-NO_2 translated to IMC-TZBCM smoothly at room temperature. The $^1H/^{13}C$ NMR and MS of IMC-TZBC-NO_2, IMC-TZBCM, IMC-FDU-TZBC-NO_2, and intermediates were well characterized (Figure S1-S32, ESI†). In the ^1H NMR of IMC-FDU-TZBC-NO_2, the signal at δ 11.79 (s, 1 H) was attributed to -CONHCO- of uracil. The signal at δ 8.14 (t, J = 6.0 Hz, 1 H) was attributed to –CONHC**H**$_2$-. The signals at δ 8.09 (d, J = 9.0 Hz, 2 H), 7.90 (s, 1 H), 7.73 (d, J = 7.2 Hz, 1 H), 7.68 (d, J = 8.4 Hz, 2 H), 7.64~7.61 (m, 3 H), 7.57 (t, J = 7.2 Hz, 1 H), 7.41 (d, J = 9.0 Hz, 2 H), 7.38 (t, J = 7.2 Hz, 1 H), 7.31 (d, J = 7.8 Hz, 1 H), 7.11 (d, J = 2.4 Hz, 1 H), 6.99 (d, J = 7.2 Hz, 1 H), 6.93 (d, J = 9.0 Hz, 1 H), 6.69 (dd, J = 7.2, 2.4 Hz, 1 H), 6.43 (dd, J = 8.4, 1.8 Hz, 1 H), 6.38 (s, 1 H), 6.05 (t, J = 6.6 Hz, 1 H) displayed characteristic of substituted 1,2,3-triazole, uracil, and benzene rings. The peak at δ 5.76 (s, 1 H) was attributed to -O**H**. The peak at δ 5.12 (s, 2 H) was attributed to -O-C**H**$_2$-Ph-NO_2. Signal at δ 4.52 (s, 2 H) was attributed to –NC**H**$_2$-1,2,3-triazole. Signal at δ 3.72 (s, 3 H) was attributed to –OC**H**$_3$. The peak at δ 3.50 (s, 2 H) was attributed to -CO-C**H**$_2$-indole. Signals at δ 3.43 (q, J = 6.6 Hz, 2 H) and 1.07 (t, J = 6.6 Hz, 3 H) were attributed to –NC**H**$_2$C**H**$_3$. Signal at δ 2.21 (s, 3 H) was attributed to –C**H**$_3$ on the indole ring. The peaks at δ 5.34 (d, J = 4.2 Hz, 1 H), 4.30 (t, J = 7.2 Hz, 2 H), 4.22~4.16 (m, 2 H), 3.94~3.92 (m, 1 H), 3.79 (q, J = 4.2 Hz, 1 H), 3.17 (d, J = 5.4 Hz, 1 H), 3.05 (q, J = 6.0 Hz, 2 H), and 1.92 (q, 3 H) were attributed to protons of aliphatic methene and methine of deoxyribose.

Scheme 2. Synthetic Routes for FDU-TZBC-NO_2, IMC-FDU-TZBC-NO_2, and IMC-TZBCM

Scheme 2

The response of IMC-FDU-TZBC-NO_2 to NTR. To verify that NTR was able to reduce the nitro group of the hypoxia trigger and consequently cleave IMC-FDU-TZBC-NO_2 and release of active drug with fluorescent dye, the absorption spectra of IMC-FDU-TZBC-NO_2 and IMC-TZBCM were delineated in Figure 1A, and a transformation experiment of IMC-FDU-TZBC-NO_2 in the presence of NTR/NADH under physiological conditions was performed, and then the mixture was monitored by fluorescence spectroscopy. IMC-TZBCM displayed a significant green fluorescence with maxima at 480 (λ_{ex}=380) nm. Nevertheless, IMC-FDU-TZBC-NO_2 solution exhibited almost no fluorescence signals because of the quenching effect of 4-nitrobenzyl group and the $\sigma_{c\text{-}c}$ bond free rotation (Figure 1B). However, the mixture solution of IMC-FDU-TZBC-NO_2 with NTR/NADH showed a same bright green fluorescence with 21-fold enhancement at same maxima at $\lambda_{ex/em}$=380/480 nm. Then, the catalytic efficiency of NTR was assessed by fluorescent spectrometry. As shown in Figure 1C and 1D, fluorescence kinetic-time curves of IMC-FDU-TZBC-NO_2 activated by NTR (at 0, 1, 2, 3, 4, 5, 6, 7, 8, 9, 10, 11, 12, 13, 14, and 15 min) indicated that the fluorescence intensity of the mixture system containing IMC-FDU-TZBC-NO_2 with NTR enhenced quickly with the prolongation of reaction time, and reached maximum when the mixture was reacted about 12 min. These results revealed that IMC-FDU-TZBC-NO_2 responded to NTRwith quickly speed and high sensitivity under hypoxia conditions.

Figure 1

Figure 1. (A) Absorbance of IMC-FDU-TZBC-NO_2 and IMC-TZBCM (50μM). (B) Fluorescence emission spectrometry were measured before and after incubation of IMC-FDU-TZBC-NO_2 with NTR/NADH (N_2 atmosphere, incubation time: 2 h, IMC-FDU-TZBC-NO_2 concentration: 50 μM, NTR concentration: 10 μg/mL, NADH concentration: 2 mM; $\lambda_{ex/em}$=380/480 nm). (C) Time-dependent fluorescence spectra, and (D) intensity of IMC-FDU-TZBC-NO_2 (concentration: 100 μM) incubation with NTR (concentration: 10 μg/mL) and NADH (concentration: 2 mM) at 37 ^{o}C under hypoxic conditions, $\lambda_{ex/em}$=380/480 nm

Mechanism of Release of Active Drug with Fluorescent Dye from IMC-FDU-TZBC-NO_2 Activated by NTR. To further confirm the mechanism of IMC-FDU-TZBC-NO_2 activated by NTR, the possibility of release of FDU with IMC-TZBCM from IMC-FDU-TZBC-NO_2 activated by $Na_2S_2O_4$ was explored. Firstly, the relative retention times of FDU, IMC-TZBCM, and IMC-FDU-TZBC-NO_2 were determined by HPLC, which were 10.930, 16.450, and 22.722 min, respectively (Figure 2A, 2B, and 2C). Then, various composition of the mixture of IMC-FDU-TZBC-NO_2 reaction with $Na_2S_2O_4$ at room temperature were analysed by comparing the retention times of various components. The peak intensity at 22.715 min corresponding to the IMC-FDU-TZBC-NO_2 was decreased, and two new strong peaks at 10.913 and 16.449 min (Figure 2D) were found, which were consistent with FDU and IMC-TZBCM matches well. These results provided an evidence for the release of FDU and IMC-TZBCM from the prodrug IMC-FDU-TZBC-NO_2. Based on above results and combined with reports,[42, 59, 60] the process of releasing FDU with IMC-TZBCM from IMC-FDU-TZBC-NO_2 is depicted as follows: firstly, under the action of $Na_2S_2O_4$ the -NO_2 group was converted to -NH_2, and IMC-FDU-TZBC-NO_2 was reduced to IMC-FDU-TZBC-NH_2. Immediately followed by a series of electron transfer process and the 1,6-rearrangement-elimination reaction, small molecule 4-methylenecyclohexa- 2,5-dien-1-iminium was eliminated, and lead to IMC-FDU-TZBC being produced. Finally, under the actions of $\sigma_{c\text{-}c}$ bond rotation of diphenyl and

intra-molecular esterification, fluorescent dye IMC-TZBCM was generated as FDU was released simultaneously (Figure 2E).

Figure 2

Figure 2. HPLC profiles of FDU(A), IMC-FDU-TZBC-NO_2 (B), IMC-TZBCM (C), and a mixture of IMC-FDU-TZBC-NO_2 with $Na_2S_2O_4$ in DMSO/H_2O (1/1, *V*/*V*) was stirred at 25 ^oC for 30 min (D), the mechanism of IMC-FDU-TZBC-NO_2 releasing FDU and IMC-TZBCM activated by hypoxia (E)

The Properties of IMC-FDU-TZBC-NO_2. To investigate conversion efficiency of IMC-FDU-TZBC-NO_2 activated by NTR, we determined the amount of released FDU from IMC-FDU-TZBC-NO_2 by HPLC method, which was incubated with NTR for different time under N_2 atmosphere. As shown in Figure 3A, with the increasing of incubation time, the amount of FDU increased correspondingly. In addition, after incubation for 12 min, the FDU release efficiency reached 73%. These results revealed that IMC-FDU-TZBC-NO_2 released FDU quickly under hypoxic conditions.

To evaluate the possible application of IMC-FDU-TZBC-NO_2 in biological systems, the selectivity of IMC-FDU-TZBC-NO_2 towards NTR over other biologically relevant some metal ions, amino acids, and biological reductants was evaluated by determination the changes of fluorescence intensity. The IMC-FDU-TZBC-NO_2 was allowed to incubate with these bio-related substances separately under N_2 atmosphere at 37 ^oC for 24 h, and then the fluorescence intensity of the mixture at $\lambda_{ex/em}$=380/480 nm was recorded. As shown in Figure 2B, IMC-FDU-TZBC-NO_2 was reduced solely by NTR to produce a strong fluorescence. However, it displayed almost no fluorescence when IMC-FDU-TZBC-NO_2 was mixed with other reductants (Vc, S^{2-}, and SO_3^{2-}), biothreitol (Cys and GSH), saccharides (Glu and Fru), amino acids (Asp, Met, and Ala), and metal ions (K^+, Zn^{2+}, Fe^{2+}, Fe^{3+}, and Cu^{2+}). This result indicated that IMC-FDU-TZBC-NO_2 exhibited unique selectivity towards NTR.

Figure 3

Figure 3. (A) The effects of incubation time on the percentage of FDU released from IMC-FDU-TZBC-NO_2 (100 μM) determined by HPLC method, which was incubated with NTR (10 μg mL^{-1}) under N_2 atmosphere. (B) The effects of various relevant species (10 μg/mL of NTR, 10 mM of GSH, Cys, Vc, Glu, Fru, Asp, Met, Ala, K^+, Zn^{2+}, Fe^{3+}, Fe^{2+}, Cu^{2+}, S^{2-}, SO_3^2) on the fluorescence intensity of IMC-FDU-TZBC-NO_2 (100 μM) in PBS buffer (containing 1% DMSO, pH 7.4, incubation time: 24 h). (C) The effects of incubation time on the fluorescence intensity of IMC-FDU-TZBC-NO_2 (100 μM) in serum solution (V_{serum} /V_{PBS}=9/1, containing 1% DMSO, pH 7.4). (D) The effects of pH values on the fluorescence intensity of IMC-FDU-TZBC-NO_2 (100 μM) and IMC-FDU-TZBC-NO_2 incubated with NTR (10 μg/mL) and NADH (2 mM) in PBS buffer (containing 1% DMSO, 10 mM) under N_2 atmosphere for 0.5 h; $\lambda_{ex/em}$= 380/480 nm. The hemolysis rate of IMC-FDU-TZBC-NO_2 (E) and FDU-TZBC-NO_2 (F) in fresh blood at different concentrations.

To assess the stability of IMC-FDU-TZBC-NO_2 in simulant physiological environment, the fluorescence changes of IMC-FDU-TZBC-NO_2 in blood serum protein solution (mixture ratio of blood serum and PBS buffer is 9 to 1) for different incubating times were measured. As shown in Figure 3C, nearly no fluorescence and negligible change were observed when the solution was stirred at 37 ^oC for 0, 4, 8, 12, 16, 20, and 24 h. It demonstrated that IMC-FDU-TZBC-NO_2 displayed remarkable stability in blood serum solution.

To further evaluate the effects of pH values on the stability of IMC-FDU-TZBC-NO_2 in PBS

solution, the fluorescence intensity of IMC-FDU-TZBC-NO_2 solution with various pH values was investigated. As shown in Figure 3D, no remarkable fluorescence and changes were observed when IMC-FDU-TZBC-NO_2 was stirred in PBS solution (In the absence of NTR) over a broad pH range of 2-12 for 0.5 h. In the presence of NTR and NADH, IMC-FDU-TZBC-NO_2 exhibited a strong green fluorescence in pH range of 4-10. The result revealed that IMC-FDU-TZBC-NO_2 showing advantageous stability in PBS solution in pH range of 2-12, and was activated by hypoxia to release IMC-TZBCM and FDU at pH range of 4 to 10.

To investigate the blood compatibility of IMC-FDU-TZBC-NO_2 and FDU-TZBC-NO_2, the hemolysis test in fresh blood was performed. As shown in Figure 3E and 3D, the hemolysis ratio of IMC-FDU-TZBC-NO_2 and FDU-TZBC-NO_2 (20 mg/mL) was less than 2%, further demonstrating the good biocompatibility, superior safe typrofile, and clear potential of IMC-FDU-TZBC-NO_2.

Based on above results, the preeminent characteristic of IMC-FDU-TZBC-NO_2 with remarkable stability under simulative physiological environments and excellent selectivity towards hypoxia endowed IMC-FDU-TZBC-NO_2 with potential application in biological media as a theranostic agent.

Cytotoxicity evaluation. To evaluate the anti-cancer effects of IMC-FDU-TZBC-NO_2, the viability of HepG-2 or BRL-3A cells co-incubation with IMC-FDU-TZBC-NO_2 under normoxia or hypoxia (3% O_2) conditions was determined *via* MTT assay, using fluorescent dye IMC-TZBCM and active drug FDU as the references. As shown in Figure 4A and 4B, for BRL-3A cells, the cell viability was decreased a little following the increasing concentration of IMC-TZBCM and IMC-FDU-TZBC-NO_2 under normoxia conditions, while the viability was decreased significantly with increasing FDU concentration (from 1 to 20 μM). The result indicated that IMC-TZBCM and IMC-FDU-TZBC-NO_2 showed negligible cytotoxicity to BRL-3A cells under normoxia conditions, while FDU showed high cytotoxicity under same conditions. For HepG-2 cells (as shown in Figure 4C and 4D), the cell viability was decreased little following the increasing concentration of IMC-TZBCM under normoxia and hypoxia (3% O_2) conditions. Nevertheless, the viability was decreased markedly with increasing FDU concentration under normoxia conditions. When IMC-FDU-TZBC-NO_2 was co-incubated with HepG-2 cells under normoxia conditions, the viability was scarcely changed with increasing IMC-FDU-TZBC-NO_2 concentration from 1 to 20 μM. When IMC-FDU-TZBC-NO_2 was co-incubated with HepG-2 cells under hypoxia (3%O_2) conditions, the cell viability was decreased obviously with increasing IMC-FDU-TZBC-NO_2 concentration from 1 to 20 μM. These results illustrated that FDU did not show hypoxia selectivity and displayed high cytotoxicity under normoxia and hypoxia conditions. However, IMC-FDU-TZBC-NO_2 exhibited high hypoxia selectivity, which displayed high cytotoxicity towards hypoxic cells, and exhibited non-cytotoxicity towards normal cells.

Figure 4

Figure 4. Cell viability of BRL-3A cells co-incubated with IMC-TZBCM, IMC-FDU-TZBC-NO_2, or FDU alone under normoxic (O_2: 20%) conditions for different time (A: 24 h; B: 48 h); Cell viability of HepG-2 cells incubated with IMC-TZBCM, IMC-FDU-TZBC-NO_2, or FDU alone under normoxic (O_2: 20%) or hypoxic (O_2: 3%) conditions for different time (C: 24 h; D: 48 h); n=10, data expressed as average ± SE, *, ** and *** means P<0.05, P<0.01 or 0.001, respectively.

Hypoxic Tumor Cell Imaging. Based on the mechanism of release of active drug with fluorescent dye simultaneously from IMC-FDU-TZBC-NO_2 activated by NTR, we monitored the hypoxia degree of cancer cells and explored the effects of the hypoxia level on the amount of

released IMC-TZBCM from IMC-FDU-TZBC-NO_2 using laser confocal microscopy. As shown in Figure 5A-D, no fluorescence signal was obtained within HepG-2 cells which were co-incubated with IMC-FDU-TZBC-NO_2 at 37 ^oC for 12 h under normoxia conditions. However, noticeable fluorescence signals were observed within HepG-2 cells which were co-incubated with IMC-FDU-TZBC-NO_2 at 37 ^oC for 12 h under various hypoxia conditions (10%, 5%, or 1% O_2). Moreover, the fluorescence intensity was enhanced with increasing hypoxia degree, and there was a certain linear relationship between the oxygen content of 20% to 1% (Figure S1). These results revealed that the rates and amounts of releasing TZ-BCM and FDU were depended on the hypoxia state within tumor cells, and the degree of hypoxia could be monitored by the intracellular fluorescence intensity. Thus, the amount of FDU release was dependent on demand of the individual patient based on the individual hypoxia state.

To evaluate the accumulation of IMC-FDU-TZBC-NO_2 in tumor hypoxia areas, HepG-2 spheres were co-incubated with IMC-FDU-TZBC-NO_2 and the fluorescence signals were measured by laser confocal microscopy. As shown in Figure 5E-G, HepG-2 spheres incubated with IMC-FDU-TZBC-NO_2 exhibited weak fluorescence on the surface and strong fluorescence in the core due to the specific feature of the tumor spheres which was closely related to the tumor microenvironment (with a normoxic surface and a hypoxic core). However, the weak fluorescence of Lyso Tracker red in the core and strong fluorescence on the surface was found due to diffusion of Lyso Tracker red. The result illustrated that the distribution and accumulation of IMC-FDU-TZBC-NO_2 was extended to the hypoxic tumor microenvironment.

Figure 5

Figure 5. Images of the HepG-2 cells co-incubated with IMC-FDU-TZBC-NO_2 under normoxic (A: 20% O_2) and different hypoxic (B: 10% O_2, C: 5% O_2, and D: 1% O_2) conditions for 12 h. Images of HepG-2 spheres co-incubated with IMC-FDU-TZBC-NO_2 and Lyso Tracker red for 12 h (E). TZ-BCM: $\lambda_{ex/em}$=380/480 nm; Lyso Tracker Red: $\lambda_{ex/em}$=577/590 nm

Targeting effects of IMC-FDU-TZBC-NO_2. Considering the superior properties of IMC-FDU-TZBC-NO_2, the cell uptake efficiency of IMC-FDU-TZBC-NO_2 dependent on IMC targeting function was explored by laser confocal microscopy. After being co-incubated with IMC (500 μM) for 12 h, the HepG-2 cells and IMC-FDU-TZBC-NO_2 (10 μM) were co-incubated for another 12 h under hypoxia conditions (5% or 1% O_2), using HepG-2 cells without co-incubation with IMC as the control. As shown in Figure 6, noticeable fluorescence was observed within HepG-2 cells which were not pretreated with IMC, and the intensity of the fluorescence signal increased with decreasing the amount of oxygen of incubator. However, the fluorescence intensity was significant decreased within HepG-2 cells which were pretreated with IMC whether the oxygen concentration was 1% or 5%, because of IMC has significantly suppressed the expression level of COX-2 which played a crucial role in tumorigenesis. These results indicated that the introduction of IMC moiety enhanced the targeting effects of IMC-FDU-TZBC-NO_2 towards cancer cells.

Figure 6

Figure 6. Images of the HepG-2 cells co-incubated with IMC-FDU-TZBC-NO_2 in absence of and in presence of IMC under hypoxic (A: 1% and B: 5%O_2) conditions for 12 h (TZ-BCM: $\lambda_{ex/em}$=380/480 nm; Lyso Tracker Red: $\lambda_{ex/em}$=577/590 nm)

Cellular uptake. Subsequently, the cellular uptake efficiency of IMC-FDU-TZBC-NO_2 by HepG-2 cells under hypoxia (1% O_2) conditions was explored. Cultured HepG2 cells were divided into four

groups. The first group, HepG2 cells were co-incubated with IMC-FDU-TZBC-NO_2 (10 μM) for 12 h under hypoxia conditions, and the fluorescence intensity of released TZ-BCM from IMC-FDU-TZBC-NO_2 was determined by flow cytometer. The second group was co-incubated with FDU-TZBC-NO_2 (10 μM) under same conditions. The third group was pretreated with IMC (500 μM) for 12 h, and then was co-incubated with IMC-FDU-TZBC-NO_2 (10 μM) for 12 h under hypoxia conditions. The fourth group without treatment with drug under same conditions was used as the control. As shown in Figure 7A and 7B, the cellular uptake efficiency of IMC-FDU-TZBC-NO_2 by HepG-2 cells was higher than that of FDU-TZBC-NO_2, and much higher than that of being pretreated with IMC. These results indicated that the IMC moiety enhanced the cellular uptake efficiency of IMC-FDU-TZBC-NO_2 by cancer cells.

Figure 7

Figure 7. The cell uptake efficiency of FDU, FDU-TZBC-NO_2, and IMC-FDU-TZBC-NO_2 by HepG-2 cells under hypoxic (1% O_2) conditions, and the cell uptake efficiency of IMC-FDU-TZBC-NO_2 by HepG-2 cells treated with IMC under hypoxic (1% O_2) conditions (λ_{ex}=480 nm)

The solubility characteristic of a prodrug is a key parameter to interpret its bioavailability. So, the lipid-water partition coefficients of FDU, FDU-TZBC-NO_2, and IMC-FDU-TZBC-NO_2 were measured by the traditional *n*-octanol–water shake flask method, and the log P values of FDU, FDU-TZBC-NO_2, and IMC-FDU-TZBC-NO_2 were calculated as -0.76, 1.67, and 2.21. The result suggested that the improved lipophilicity of IMC-FDU-TZBC-NO_2 due to the binding of hypoxic trigger, fluorescent dye precursor, and targeting moiety. In addition, hypoxia targeted drug delivery is difficult because hypoxic areas in tumors are often poorly vascularized (that's one of the reasons why it is hypoxic), together with the fact that tumors are in general highly stromal,[61] the challenge of FDU with poor tumor penetration due to the low lipophilicity could be dramatically increased by prodrug of FDU with improved lipophilicity as Wang reported.[62] Therefore, the tumor penetration of FDU IMC-FDU-TZBC-NO_2 was improved by its enhanced lipophilicity due to the binding of hypoxic trigger, fluorescent dye precursor, and targeting moiety.

***In vivo* antitumor activity.** Due to its significant cytotoxicity to hypoxia cancer cells, the *in vivo* evaluation of prodrug IMC-FDU-TZBC-NO_2 against xenograft mice vaccinated with HepG-2 cells was investigated. Mice were intravenously tail vein-injected with IMC-FDU-TZBC-NO_2, FDU-TZBC-NO_2 and PBS (control group) at a dose of 10 mg/kg every 3 days with an intermittent q^2d*7 schedule, respectively. The tumor volumes of groups that were injected with FDU-TZBC-NO_2 or IMC-FDU-TZBC-NO_2 were recorded. As shown in Table S1 and Figure 8, compared with the control, both IMC-FDU-TZBC-NO_2 and FDU-TZBC-NO_2 inhibited HepG-2 tumor growth comparing with the control group, showing low toxicity with no magic weight loss during the treatment process (Figure 8A and 8B). It is worth noting that according to the experimental results, the tumor inhibition rate of IMC-FDU-TZBC-NO_2 (82.7%) is significantly higher than that of FDU-TZBC-NO_2 (51%), which may be due to the targeting effect of IMC. In addition, the photograph of the resected tumours from representative mice intuitively demonstrated that the tumor sizes of mice injected with IMC-FDU-TZBC-NO_2 group were much smaller than that of injected with FDU-TZBC-NO_2 and PBS (Figure 8C and 8D), which could be attributed to the IMC moiety enhancing the targeting and cellular uptake efficiency of IMC-FDU-TZBC-NO_2 combination with the release of the FDU induced by hypoxia. Meanwhile, to investigate the toxicity of FDU-TZBC-NO_2 and IMC-FDU-TZBC-NO_2, mice body weight was measured during the treatment

period. As shown in Figure 8B, the body weight having no obvious change indicated that FDU-TZBC-NO_2 and IMC-FDU-TZBC-NO_2 had almost no toxicity in mice produced during the 22 days treatments. The TUNEL staining exhibited much more destruction within tumor tissue of mice treated with IMC-FDU-TZBC-NO_2 than that of treated with FDU-TZBC-NO_2 due to the IMC moiety improving the efficiency of tumor-targeting and the cellular uptake efficiency of IMC-FDU-TZBC-NO_2 (Figure 8E). These results demonstrated that the IMC-guided and hypoxia-activated IMC-FDU-TZBC-NO_2 was a prodrug for solid cancer chemotherapy with high efficacy and low side effects.

Figure 8

Figure 8. The relative tumor volume normalized to initial volume (A), body weight (B), and average tumor weight changes (C) in 22 days after various treatments (injected with IMC-FDU-TZBC-NO_2, FDU-TZBC-NO_2, or PBS; n= 5, data expressed as average ± SE, *, ** and *** means $P<0.05$, $P<0.01$ or 0.001, respectively). Representative histological photomicrograph (D) of HepG-2-cell-inoculated xenograft mice injected with IMC-FDU-TZBC-NO_2, FDU-TZBC-NO_2, and PBS (Control). TUNEL stained images of cancer tissues from the HepG-2-cell-inoculated xenograft mice after various treatments for 22 days (E).

Besides, to assess the systemic toxicity of IMC-FDU-TZBC-NO_2 *in vivo*, a further histological study was conducted on tumor and major organs through hematoxylin and eosin (H&E) staining. As shown in Figure 9, compared with the groups treated with FDU-TZBC-NO_2 and PBS, the mice treated with IMC-FDU-TZBC-NO_2 exhibited significantly more apoptotic cells in tumor tissue. Moreover, the major organs like the heart, spleen, kidney, liver, and lung of xenograft mice vaccinated with HepG-2 cells had almost same morphologies to the control group, suggested that IMC-FDU-TZBC-NO_2 displayed no notable side effect on the major organs of mice. However, starting from the 22^{th} day, tumor-bearing mice in the control group began to die off. Taken together, IMC-FDU-TZBC-NO_2 could achieve high inhibition effect to tumor growth and no side effect on normal organs, due to the integration of the targeting strategy and prodrug activated by hypoxia.

Figure 9

Figure 9. H&E staining of the sacrificed cancer tissues and major organs after various treatments for 22 d

■ CONCLUSION

In conclusion, a new theranostic prodrug IMC-FDU-TZBC-NO_2 based on COX-2 inhibitor IMC-guiding combination hypoxia-activation for targeted chemotherapy, releasing drug on-demand, combination therapy under the guidance of imaging was developed. IMC-FDU-TZBC-NO_2 showed a high targeting specificity to tumor cells, a specificand predominant imaging property to hypoxia microenvironment, and excellent stability in physiological solutions. Furthermore, the IMC moiety improved the cellular uptake efficiency of IMC-FDU-TZBC-NO_2. In addition, the hypoxia response group enhanced the hypoxic selectivity towards hypoxic tumor cells and reduced the cytotoxicity to normal cells. Eventually, IMC-FDU-TZBC-NO_2 showed significant inhibition tumor growth of mice in xenograft mice vaccinated with HepG-2 cells, exhibited no toxic side effects on heart, liver, spleen, lung and kidney. This strategy will offer a platform for design a hypoxia-activated and tumor-targeted anticancer theranostic agent for

targeted chemotherapy, releasing active drug based on hypoxic status, non-invasive and the real-time monitoring of hypoxia and active drug release, inhibition tumor growth with high efficiency and no side effects. To improve the diagnostic effect, the future research of our group should be to improve the strategy of monitoring of hypoxia and active drug release which will be operated in the near infrared wavelength.

■ EXPERIMENTAL SECTION

Materials. 4-Bromo-3-methoxyaniline, 4-nitrobenzyl bromide, hydrochloride, 2-ethoxycarbonylbenzeneboronic acid, 3-bromopropyne, floxuridine (FDU), 4-dimethylaminopyridine (DMAP), *N,N*'-diisopropyl carbodiimide (DIC), 2-(7-aza-1H-benzotriazole-1-yl)-1,1,3,3-tetramethyluronium hexafluorophosphate (HATU), tetrakis(triphenylphosphine)palladium, 1-amino-3-chloropropane, and IMC were purchased form Energy Chemical (Shanghai, China). Potassium carbonate, sodium carbonate, sodium sulfate, copper sulfate pentahydrate, ammonium chloride, sodium dithionate, sodium hydroxide, petroleum ether (PE), methanol (MeOH), ethyl acetate (EA), ethyl ether, 1,4-dioxane, tetrahydrofuran (THF), *N,N*-dimethylformamide (DMF), acetonitrile (ACN), dichloromethane (DCM), dimethyl sulfoxide (DMSO), concentrated hydrochloric acid, and concentrated sulfuric acid were all commercially available analytically which were purchased from Tianjin Kemiou Chemical Reagent Co. Ltd. (Tianjin, China). *L*-Ascorbic acid (Vc), *L*-cysteine, *L*-glutamic acid, and *L*-alanine were obtained from Alfa Aesar Chemical Co. Ltd. (Shanghai, China). Nicotinamide adenine dinucleotide (NADH) and sodium azide (NaN_3) were purchased from Sigma-Aldrich Co. LLC (USA). Indomethacin (IMC), trifluoroacetic acid (TFA), benzyl penicillin, streptomycin, thiazolyl blue tetrazolium bromide (MTT), and NTR (≥100 units/mg) were purchased from Sigma Chemical Co (USA). Lyso Tracker Red was obtained from Life Technology (New York, USA). BRL-3A and HepG-2 cell lines were obtained from Beijing Union Cell Resource Center (China). Immunodeficient BALB/c (nu/nu) mice (four-weeks-old) were achieved from Weitong Lihua Experimental Animal Technology Co Ltd (Beijing, China).

Instrumentation. NMR was measured on a Bruker AVANCEIII Spectrometer (Germany). MS was measured on a 4000 QTRAP LC-MS (USA). IR was performed on a spectrophotometer (Thermo Scientific Nicolet iS10, USA). Fluorescence measurements were performed on a Fluorescence Spectrophotometer (Hitachi F-7000, Japan). The absorbance was measured on a Bio-Rad Model 680 microplate spectrophotometer (USA). The relative retention time was measured on a HPLC system (Agilent 1260, USA), which was equipped with quaternary G1311C pump, HC-C18 (Agilent, 250 mm × 4.6 mm, 5 μm), and G1314F UV-vis detector. Fluorescence imaging was measured on an LSM 880 Confocal Microscope (Germany). Cellular uptake was checked by a FACS-Calibur Flow Cytometer (BD Biosciences, USA).

Synthesis of 4-bromo-*N*-ethyl-3-methoxyaniline (1). 4-Bromo-3-methoxyaniline (5.01 g, 24.75 mmol), dry DMF (30 mL), bromoethane (3.10 g, 28.46 mmol), and K_2CO_3 (10.26 g, 74.24 mmol) were heated to 100 °C for 14 h. Followed by cooling and being poured into 50 mL of water, the mixture was extracted with EA (50 mL × 3), washed with saline (50 mL ×3), and dried with Na_2SO_4 sequentially. Then, EA was removed, and compound **1** was isolated as yellow liquid (2.51 g, 44% yield) from the crude by column chromatography isolation (V_{EA}/V_{PE}=1/50). ^{1}H NMR (600 MHz, DMSO-d_6, ppm): δ 7.16 (d, J = 8.4 Hz, 1 H), 6.27 (d, J = 2.4 Hz, 1 H), 6.09 (dd, J = 9.0, 2.4 Hz, 1 H), 5.74 (s, 1 H), 3.75 (s, 3 H), 3.02 (m, 2 H), 1.15 (t, J = 7.2 Hz, 3 H). ^{13}C NMR (150 MHz, $CDCl_3$, ppm): δ 156.41, 149.16, 133.29, 106.06, 98.16, 97.44, 55.98, 38.58, 14.72. MS (*m/z*): Calcd. for

$C_9H_{12}BrNO$, 230.0 $[M+H]^+$; Found, 229.8.

Synthesis of 2-bromo-5-(ethylamino) phenol (2). Compound **1** (3.02 g, 13.04 mmol), boron tribromide (6.53 g, 26.08 mmol), and dry DCM (20 mL) were stirred for 2 h at 30 °C. After being added 50 mL of water and adjusted to pH 7 with Na_2CO_3 (aq.), the obtained mixture was extracted with DCM (50 mL × 3), and dried with $MgSO_4$. Then, DCM wasremoved, and compound **2** was generated as white solid (2.23 g, 79% yield) from the crude by column chromatography isolation (V_{EA}/V_{PE}=1/30). Mp: 95.7-96.2 °C. ^{1}H NMR (600 MHz, DMSO-d_6, ppm): δ 9.63 (s, 1 H), 7.06 (d, J = 8.4 Hz, 1 H), 6.17 (d, J = 2.4 Hz, 1 H), 5.98 (dd, J = 8.6, 2.4 Hz, 1 H), 5.59 (t, J = 7.2 Hz, 1 H), 2.93 (m, 2 H), 1.13 (t, J = 7.2 Hz, 3 H). ^{13}C NMR (150 MHz, $CDCl_3$, ppm): δ 152.90, 149.56, 131.89, 107.34, 99.61, 96.79, 38.47, 14.67. MS (*m/z*): Calcd. for $C_8H_{10}BrNO$, 216.0 $[M+H]^+$; Found, 215.9.

Synthesis of *t*-butyl (4-bromo-3-hydroxyphenyl)ethyl carbamate (3). Boc anhydride (3.94 g, 18.05 mmol), 1,4-dioxane (20 mL), and compound **2** (3.00 g, 13.88 mmol) were stirred for 24 h at 35 °C. After drying, compound **3** was generated as white solid (3.07 g, 70% yield) from the residue by column chromatography isolation (V_{EA}/V_{PE}=1/30). Mp: 106.0-106.6 °C. ^{1}H NMR (600 MHz, $CDCl_3$, ppm): δ 7.39 (d, J = 8.4 Hz, 1 H), 6.88 (s, 1 H), 6.68 (d, J = 8.4 Hz, 1 H), 5.57 (s, 1 H), 3.64 (q, J = 7.2 Hz, 2 H), 1.44 (s, 9 H), 1.14 (t, J = 7.2 Hz, 3 H). ^{13}C NMR (150 MHz, $CDCl_3$, ppm): δ 154.40, 152.66, 143.14, 131.86, 120.38, 114.94, 107.30, 80.57, 44.95, 28.33, 13.79. MS (*m/z*): Calcd. for $C_{13}H_{18}BrNO_3$, 338.1 $[M+Na]^+$; Found, 338.2.

Synthesis of *t*-butyl (4-bromo-3-((4-nitrobenzyl)oxy)phenyl)ethyl carbamate (4). Compound **3** (5.00 g, 15.81 mmol), 4-nitrobenzyl bromide (5.12 g, 23.72 mmol), dry ACN (20 mL), and K_2CO_3 (6.57 g, 47.46 mmol) were refluxed for 3 h. After ACN being removed, compound **4** was generated as yellow solid (5.69 g, 80% yield) from the residue by column chromatography isolation (V_{EA}/V_{PE}=1/20). Mp: 127.4-128.2 °C. ^{1}H NMR (600 MHz, $CDCl_3$, ppm): δ 8.27 (d, J = 8.4 Hz, 2 H), 7.69 (d, J = 8.4 Hz, 2 H), 7.53 (d, J = 8.4 Hz, 1 H), 6.83 (s, 1 H), 6.75 (d, J = 8.4 Hz, 1 H), 5.22 (s, 2 H), 3.63 (q, J = 7.2 Hz, 2 H), 1.43 (s, 9 H), 1.12 (t, J = 7.2 Hz, 3 H). ^{13}C NMR (150 MHz,$CDCl_3$, ppm): δ 154.41, 154.10, 147.68, 143.69, 143.02, 133.21, 127.45, 123.86, 121.05, 113.11, 109.45, 80.49, 69.65, 44.97, 28.35, 13.89.

Synthesis of ethyl 4'-((*t*-butoxycarbonyl)ethylamino)-2'-((4-nitrobenzyl)oxy)-1,1'-biphenyl-2-carboxylate (5). Tetrakis(triphenylphosphine)palladium (1.01 mg, 0.87 mmol), compound **4** (2.40 g, 5.33 mmol), 2-ethoxycarbonylbenzeneboronic acid (1.25 g, 6.40 mmol), $NaHCO_3$ (1.34 g, 16.00 mmol), and 25 mL of H_2O/DMF (1/4) were heated to 120 °C and stirred for 4 h under N_2. After solvent being removed, compound **5** was isolated as yellow solid (1.86 g, 67% yield) from the residue by column chromatography isolation (V_{EA}/V_{PE} =1/15). Mp: 113.5-114.1 °C. ^{1}H NMR (600 MHz,$CDCl_3$, ppm): δ 8.13 (d, J = 7.8 Hz, 2 H), 7.94 (d, J = 7.8 Hz, 1 H), 7.56 (t, J = 7.2 Hz, 1 H), 7.45 (t, J = 7.2 Hz, 1 H) 7.33 (d, J = 8.4 Hz, 3 H), 7.23 (d, J = 8.4 Hz, 1 H), 6.93 (d, J = 7.8 Hz, 1 H), 6.82 (s, 1 H), 5.05 (s, 2 H), 4.04 (s, 2 H), 3.69 (q, J = 7.2 Hz, 2 H), 1.46 (s, 9 H), 1.18 (t, J = 7.2 Hz, 3 H), 0.98 (t, J = 7.2 Hz, 3 H). ^{13}C NMR (150 MHz, $CDCl_3$, ppm): δ 167.94, 154.79, 154.36, 147.35, 144.26, 143.05, 138.29, 131.82, 131.51, 131.38, 129.99, 129.71, 129.56, 127.40, 127.13, 123.54, 119.80, 111.70, 80.20, 69.42, 60.57, 45.17, 28.39, 13.98, 13.76. MS (*m/z*): Calcd. for $C_{29}H_{32}N_2O_7$, 543.2 $[M+Na]^+$; Found, 542.4.

Synthesis of ethyl 4'-(ethylamino)-2'-((4-nitrobenzyl)oxy)-1,1'-biphenyl-2-carboxylate (6). Compound **5** (3.00 g, 5.77 mmol), hydrochloric acid (10 mL), and 1,4-dioxane (20 mL) were stirred for 4 h at 35 °C. After being dispersed into 100 mL of water and adjusted to pH 8 with

Na_2CO_3 (aq.), the resulting solution was extracted with DCM (50 mL × 3), washed with saline (50 mL × 3), and dried with $MgSO_4$ sequentially. Then, DCM was removed, and compound **6** was obtained as orange solid (1.87 g, 77% yield) from the residue by column chromatography isolation (V_{EA}/V_{PE}=1/10). Mp: 135.1-135.9 °C. ^{1}H NMR (600 MHz, DMSO-d_6, ppm): δ 8.15 (d, J = 9.0 Hz, 2 H), 7.69 (d, J = 7.8 Hz, 1 H), 7.55 (t, J = 7.8 Hz, 1 H), 7.48 (d, J = 8.4 Hz, 2 H), 7.37 (t, J = 7.8 Hz, 1 H), 7.31 (d, J = 7.2 Hz, 1 H), 6.91 (d, J = 9 Hz, 1 H), 6.24 (d, J = 7.2 Hz, 2 H), 5.65 (t, J = 5.4 Hz, 1 H), 5.10 (s, 2 H), 3.97 (q, J = 7.2 Hz, 2 H), 3.05 (m, 2 H), 1.14 (t, J = 7.2 Hz, 3 H), 0.94 (t, J = 7.2 Hz, 3 H). ^{13}C NMR (150 MHz, DMSO-d_6, ppm): δ 167.86, 155.33, 149.97, 146.73, 145.33, 138.80, 131.90, 131.31, 131.15, 130.42, 128.75, 127.50, 126.13, 123.23, 117.87, 104.71, 96.82, 68.20, 59.99, 37.33, 14.35, 13.60. MS (*m/z*): Calcd. for $C_{24}H_{24}N_2O_5$, 421.2 $[M+H]^+$; Found, 421.4.

Synthesis of ethyl 4'-(ethyl(prop-2-yn-1-yl)amino)-2'-((4-nitrobenzyl)oxy)-1,1'-biphenyl-2-carboxylate (7). Compound **6** (2.00 g, 4.76 mmol), propargyl bromide (0.85 g, 7.15 mmol), dry ACN (20 mL), and 1.97 g of K_2CO_3 (14.28 mmol) were stirred for 12 h at 60 °C. Then, K_2CO_3 and ACN were removed sequentially, and compound **7** was generated as yellow-brown solid (873 mg, 40% yield) from the residue by column chromatography isolation (V_{EA}/V_{PE}=1/20). Mp: 104.8-105.7 °C. ^{1}H NMR (600 MHz, DMSO-d_6, ppm): δ 8.15 (d, J = 8.4 Hz, 2 H), 7.73 (d, J = 7.8 Hz, 1 H), 7.57 (t, J = 7.2 Hz, 1 H), 7.48 (d, J = 8.4 Hz, 2 H), 7.40 (t, J = 7.2 Hz, 1 H), 7.34 (d, J = 7.8 Hz, 1 H), 7.03 (d, J = 8.4 Hz, 1 H), 6.47 (d, J = 8.4 Hz, 1 H), 6.44 (s, 1 H), 5.17 (s, 2 H), 4.10 (s, 2 H), 3.97 (q, J = 7.2 Hz, 2 H), 3.42 (q, J = 7.2 Hz, 2 H), 3.06 (s, 1 H), 1.10 (t, J = 7.2 Hz, 3 H), 0.92 (t, J = 7.2 Hz, 3 H). ^{13}C NMR (150 MHz, $CDCl_3$, ppm): δ 168.39, 155.69, 148.67, 147.29, 144.87, 138.94, 132.00, 131.55, 131.31, 130.77, 129.53, 127.22, 126.66, 123.53, 121.13, 107.05, 99.34, 71.79, 69.51, 65.56, 60.51, 45.85, 39.76, 13.86, 12.47. MS (*m/z*): Calcd. for $C_{27}H_{26}N_2O_5$, 459.2 $[M+H]^+$; Found, 459.7.

Synthesis of 4'-(ethyl(prop-2-yn-1-yl)amino)-2'-((4-nitrobenzyl)oxy)-1,1'-biphenyl-2-carboxylic acid (8). Compound **7** (500 mg, 1.09 mmol) dissolved in 4 mL of 1,4-dioxane and 30% sulfuric acid (20 mL) were heated at 100 °C for 12 h. Then, the mixture was cooled down, dispersed into 50 mL of water, adjusted to pH 6 with Na_2CO_3 (aq), extracted with DCM (50 mL × 3), washed with saline (50 mL ×3), and dried with $MgSO_4$ sequentially. After DCM being removed, compound **8** was afforded as yellow solid (235 mg, 50 % yield) from residue by column chromatography isolation (V_{MeOH}/V_{DCM}=1/80). Mp: 191.5-192.2 °C. ^{1}H NMR (600 MHz, DMSO-d_6, ppm): δ 12.35 (s, 1 H), 8.15 (d, J = 8.4 Hz, 2 H), 7.74 (d, J = 7.8 Hz, 1 H), 7.55 (d, J = 9 Hz, 2 H), 7.52 (d, J = 7.2 Hz, 1 H), 7.37 (t, J = 7.8 Hz, 1 H), 7.30 (d, J = 7.2 Hz, 1 H), 7.02 (d, J = 8.4 Hz, 1 H), 6.44 (dd, J_1 = 8.4 Hz, J_2 = 2.4 Hz, 1 H), 6.38 (d, J = 1.8 Hz, 1 H), 5.19 (s, 2 H), 4.08 (d, J = 1.8 Hz, 2 H), 3.39 (q, J = 7.2 Hz, 2 H), 3.07 (s, 1 H), 1.08 (t, J = 7.2 Hz, 3 H). ^{13}C NMR (150 MHz, DMSO-d_6, ppm): δ 169.02, 155.55, 148.09, 146.71, 145.50, 138.29, 132.87, 131.42, 130.75, 130.42, 128.86, 127.71, 126.29, 123.29, 119.55, 105.70, 98.38, 81.03, 73.99, 68.64, 44.84, 38.85, 12.13. MS (*m/z*): Calcd. for $C_{25}H_{22}N_2O_5$, 431.2 $[M+H]^+$; Found, 431.3.

Synthesis of FDU-TZBC-NO_2. Compound **8** (81 mg, 0.19 mmol), dry DMF (0.5 mL), DMAP (10 mg, 0.07 mmol), DIC (94 mg, 0.74 mmol), and FDU (46 mg, 0.19 mmol) were heated to 50 °C and stirred for 24 h. After being cooled down and dispersed into 5 mL of water, the obtained mixture was extracted with DCM (5 mL ×4), washed with saline (5 mL×4), and dried with $MgSO_4$ sequentially. Then, DCM was removed, and FDU-TZBC-NO_2 was afforded as yellow-green solid (22 mg, 18% yield) from the residue by column chromatography isolation (V_{MeOH}/V_{DCM}=1/50). Mp: 91.5-92.2 °C. ^{1}H NMR (600 MHz, DMSO-d_6, ppm): δ 11.78 (s, 1 H), 8.11 (d, J = 9 Hz, 2 H), 7.75

(d, *J* = 7.8 Hz, 1 H), 7.65 (d, *J* = 6.6 Hz, 1 H), 7.59 (t, *J* = 7.2 Hz, 1 H), 7.45 (d, *J* = 9 Hz, 2 H), 7.40 (t, *J* = 7.8 Hz, 1 H), 7.35 (d, *J* = 7.8 Hz, 1 H), 7.05 (d, *J* = 8.4 Hz, 1 H), 6.47 (dd, J_1 = 8.4 Hz, J_2 = 2.4 Hz, 1 H), 6.42 (s, 1 H), 6.06 (t, *J* = 7.2 Hz, 1 H), 5.31 (d, *J* = 4.8 Hz, 1 H), 5.16 (s, 2 H), 4.21 (s, 2 H), 4.10 (s, 2 H), 3.99 (m, 1 H), 3.79 (q, *J* = 4.8 Hz, 1 H), 3.42 (q, *J* = 7.2 Hz, 2 H), 3.07 (s, 1 H), 2.01 (m, 2 H), 1.10 (t, *J* = 7.2 Hz, 3 H). ^{13}C NMR (150 MHz, DMSO-d_6, ppm): δ 167.47, 156.79, 155.27, 148.81, 148.41, 146.68, 145.18, 140.61, 139.08, 138.36, 131.61, 131.48, 131.12, 130.37, 128.93, 127.51, 126.48, 124.28, 123.24, 118.80, 106.00, 98.34, 84.37, 83.74, 80.96, 74.00, 70.09, 68.44, 64.33, 44.87, 38.94, 12.08. MS (*m/z*): Calcd. for $C_{34}H_{31}FN_4O_9$, 687.2 $[M+K]^+$; Found, 697.8.

Synthesis of IMC-N_3. 1-Amino-3-chloropropane hydrochloride (100 mg, 0.77 mmol), NaN_3 (50 mg, 0.77 mmol), and water (3 mL) were refluxed for 16 h. Then, the solution was cooled down, neutralized with NaOH (aq), extracted with Et_2O (2 mL × 3), and dried with K_2CO_3. Fellowed by Et_2O being evaporated, $NH_2CH_2CH_2CH_2N_3$ was obtained aslight yellow oily liquid (69 mg, 90% yield).

IMC (500 mg, 1.40 mmol), HATU (638 mg, 1.68 mmol), and dry DMF (10 mL) were stirred at 35 ^{o}C for 1 h. Followed by adding $NH_2CH_2CH_2CH_2N_3$ (127 mg, 1.27 mmol), the solution was stirred for another 1 h. After being dispersed into 100 mL of water, the obtained mixture was extracted with EA (50 mL ×3), washed with saline (50 mL ×3), and dried with $MgSO_4$ sequentially. Fellowed by EA being removed, IMC-N_3 was obtained as light green solid (223 mg, 40% yield) from the crude by column chromatography isolation (Eluent:V_{EA}/V_{PE}=1/5). Mp: 159.3-160.5 °C. ^{1}H NMR (600 MHz, $CDCl_3$, ppm): δ 7.64 (d, *J* = 8.4 Hz, 2 H), 7.48 (d, *J* = 8.4 Hz, 2 H), 6.89 (d, *J* = 2.4 Hz, 1 H), 6.85 (d, *J* = 9.0 Hz, 1 H), 6.70 (dd, J_1 = 9.0 Hz, J_2 = 2.4 Hz, 1 H), 5.89 (s, 1 H), 3.82 (s, 3 H), 3.64 (s, 2 H), 3.29 (q, *J* = 6.6 Hz, 2 H), 3.26 (t, *J* = 6.6 Hz, 2 H), 2.39 (s, 3 H), 1.70 (m, 2 H). ^{13}C NMR (150 MHz, $CDCl_3$, ppm): δ 170.07, 168.33, 156.33, 139.61, 136.42, 133.56, 131.18, 130.93, 129.24, 128.84, 115.15, 112.74, 112.28, 100.83, 55.77, 49.47, 37.46, 32.22, 28.60, 13.22. MS (*m/z*): Calcd. for $C_{23}H_{23}ClN_4O_3$, 461.2 $[M+Na]^+$; Found, 462.1.

Synthesis of IMC-TZBC-NO_2. Compound **8** (215 mg, 0.5 mmol), IMC-N_3 (220 mg, 0.5 mmol), 6 mL of THF, and $CuSO_4$•$5H_2O$ (71 mg, 0.28 mmol) dissolved in water (3 mL) were stirred at rt for 5 min. Followed by adding 3 mL of Vc (50 mg, 0.28 mmol) solution, the mixture was heated to 55 ^{o}C and stirred for 10 h under N_2. After being cooled down, the resulting mixture was dispersed into 100 mL of NH_4Cl (aq), extracted by EA (80 mL × 3), washed twice with 50 mL of saline, and dried with $MgSO_4$ sequentially. Fellowed by EA being removed, IMC-TZBC-NO_2 was afforded as yellow-brown solid (243 mg, 70% yield) from the residue by column chromatography isolation (V_{MeOH}/V_{DCM}=1/50). Mp: 215.2-215.8 °C. ^{1}H NMR (600 MHz, DMSO-d_6, ppm): δ 12.29 (s, 1 H), 8.12 (d, *J* = 8.4 Hz, 2 H), 8.09 (d, *J* = 5.4 Hz, 1 H), 7.90 (s, 1 H), 7.72 (d, *J* = 7.2 Hz, 1 H), 7.67 (d, *J* = 8.4 Hz, 2 H), 7.63 (d, *J* = 8.4 Hz, 2 H), 7.51 (d, *J* = 9 Hz, 2 H), 7.49 (d, *J* = 7.2 Hz, 1 H), 7.35 (t, *J* = 7.8 Hz, 1 H), 7.26 (d, *J* = 7.8 Hz, 1 H), 7.10 (d, *J* = 2.4 Hz, 1 H), 6.97 (d, *J* = 8.4 Hz, 1 H), 6.93 (d, *J* = 9 Hz, 1 H), 6.69 (dd, *J* = 9 Hz, 2.4 Hz, 1 H), 6.42 (dd, *J* = 8.4, 1.8 Hz, 1 H), 6.36 (s, 1 H), 5.14 (s, 2 H), 4.49 (s, 2 H), 4.30 (t, *J* = 7.2 Hz, 2 H), 3.72 (s, 3 H), 3.50 (s, 2 H), 3.41 (q, *J* = 7.2 Hz, 2 H), 3.05 (q, *J* = 6.6 Hz, 2 H), 2.21 (s, 3 H), 1.92 (m, 2 H), 1.06 (t, *J* = 7.2 Hz, 3 H). ^{13}C NMR (150 MHz, DMSO-d_6, ppm): δ 169.56, 169.27, 167.80, 155.54, 155.47, 148.40, 146.66, 145.52, 144.69, 138.35, 137.54, 135.13, 134.21, 132.76, 131.37, 131.09, 130.83, 130.74, 130.53, 130.28, 128.99, 128.85, 127.64, 126.15, 123.24, 122.73, 118.50, 114.53, 114.21, 111.22, 104.77, 101.78, 97.32, 68.40, 55.38, 47.09, 44.90, 44.44, 35.99, 31.14, 29.94, 13.31, 12.06. MS (*m/z*): Calcd. for $C_{47}H_{44}ClN_7O_8$, 892.3 $[M+Na]^+$; Found, 893.0.

Synthesis of IMC-FDU-TZBC-NO_2. IMC-TZBC-NO_2 (102 mg, 0.11 mmol), DMAP (6 mg, 0.05 mmol), DIC (54 mg, 0.43 mmol), FDU (28 mg, 0.11 mmol), and dry DMF (1 mL) were heated to 50 ^oC and stirred for 24 h. After cooling and adding 5 mL of water, the obtained mixture was extracted with DCM (5 mL × 3), washed with saline (5 mL× 2), and dried with $MgSO_4$. Then, DCM was removed, IMC-FDU-TZBC-NO_2 was afforded as yellow-green solid (20 mg, 16% yield) from the crude by column chromatography isolation (Eluent: V_{MeOH}/V_{DCM}=1/40). Mp: 130.9-132.4 °C. ^{1}H NMR (600 MHz, DMSO-d_6, ppm): δ 11.79 (s, 1 H), 8.14 (t, *J* = 6 Hz, 1 H), 8.08 (d, *J* = 9.0 Hz, 2 H), 7.91 (s, 1 H), 7.73 (d, *J* = 7.2 Hz, 1 H), 7.68 (d, *J* = 8.4 Hz, 2 H), 7.63 (d, *J* = 8.4 Hz, 3 H), 7.57 (t, *J* = 7.2 Hz, 1 H), 7.42 (d, *J* = 9.0 Hz, 2 H), 7.38 (t, *J* = 7.2 Hz, 1 H), 7.31 (d, *J* = 7.8 Hz, 1 H), 7.11 (d, *J* = 2.4 Hz, 1 H), 6.99 (d, *J* = 7.2 Hz, 1 H), 6.93 (d, *J* = 9 Hz, 1 H), 6.69 (dd, J_1 = 7.2 Hz, J_2 = 2.4 Hz, 1 H), 6.43 (dd, *J* = 8.4, 1.8 Hz, 1 H), 6.38 (s, 1 H), 6.06 (t, *J* = 6.6 Hz, 1 H), 5.34 (d, *J* = 4.2 Hz, 1 H), 5.12 (s, 2 H), 4.52 (s, 2 H), 4.30 (t, *J* = 7.2 Hz, 2 H), 4.19 (m, 2 H), 3.93 (m, 1 H), 3.79 (q, *J* = 4.2 Hz, 1 H), 3.72 (s, 3 H), 3.50 (s, 2 H), 3.43 (q, *J* = 7.2 Hz, 2 H), 3.17 (d, *J* = 5.4 Hz, 1 H), 3.05 (q, *J* = 6.6 Hz, 2 H), 2.21 (s, 3 H), 1.92 (m, 3 H), 1.07 (t, *J* = 7.2 Hz, 3 H). ^{13}C NMR (150 MHz, DMSO-d_6, ppm): δ 167.80, 167.60, 155.53, 155.33, 148.80, 148.63, 146.59, 145.18, 144.67, 140.57, 139.03, 138.33, 137.53, 135.09, 134.17, 131.54, 131.37, 131.10, 131.07, 130.82, 130.24, 128.97, 127.44, 126.31, 123.17, 122.74, 117.74, 114.50, 114.26, 111.25, 101.72, 97.18, 84.36, 83.79, 70.10, 68.34, 64.29, 60.32, 55.33, 48.54, 47.10, 44.98, 44.47, 35.96, 34.62, 31.08, 29.90, 18.57, 13.77, 13.28, 11.98.

Synthesis of IMC-TZBCM. 4 mL of $Na_2S_2O_4$ (200 mg, 1.15 mmol) solution, IMC-TZBC-NO_2 (200 mg, 0.23 mmol), DCM (2 mL), and MeOH (10 mL) were stirred for 2 h at rt. After being dispersed into 50 mL of water, the resulting mixture was extracted with DCM (40 mL ×4), washed with saline (40 mL × 3), and dried with $MgSO_4$ sequentially. Then, DCM was removed, IMC-TZBCM was generated as yellow green solid (138 mg, 84% yield) from the crude by column chromatography isolation (V_{MeOH}/V_{DCM}=1/100). Mp: 169.2-170.1 °C. ^{1}H NMR (600 MHz, DMSO-d_6, ppm): δ 8.60 (d, *J* = 7.8 Hz, 1 H), 8.13 (d, *J* = 7.8 Hz, 1 H), 8.08 (t, *J* = 5.4 Hz, 1 H), 8.05 (d, *J* = 9.0 Hz, 1 H), 7.99 (s, 1 H), 7.82 (t, *J* = 7.8 Hz, 1 H), 7.67 (d, *J* = 8.4 Hz, 2 H), 7.63 (d, *J* = 8.4 Hz, 2 H), 7.47 (t, *J* = 7.8 Hz, 1 H), 7.09 (d, *J* = 2.4 Hz, 1 H), 6.93 (d, *J* = 9 Hz, 1 H), 6.85 (dd, *J* = 9, 2.4 Hz, 1 H), 6.71 (s, 1 H), 6.68 (dd, *J* = 9, 2.4 Hz, 1 H), 4.63 (s, 2 H), 4.31 (t, *J* = 7.2 Hz, 2 H), 3.72 (s, 3 H), 3.56 (q, *J* = 7.2 Hz, 2 H), 3.48 (s, 2 H), 3.05 (q, *J* = 6.6 Hz, 2 H), 2.21 (s, 3 H), 1.93 (m, 2 H), 1.16 (t, *J* = 7.2 Hz, 3 H). ^{13}C NMR (150 MHz, DMSO-d_6, ppm): δ 174.75, 173.05, 166.13, 160.78, 159.48, 157.80, 154.88, 149.32, 142.77, 140.83, 140.35, 139.46, 136.34, 136.06, 135.52, 134.23, 128.20, 128.06, 126.33, 123.55, 119.75, 119.47, 116.48, 114.78, 111.09, 107.06, 106.98, 103.74, 92.33, 60.62, 52.41, 50.08, 49.95, 41.24, 36.38, 35.18, 18.56, 17.29. MS (*m/z*): Calcd. for $C_{40}H_{37}ClN_6O_5$, 717.3 $[M+H]^+$; Found, 717.0.

Fluorescence measurements of IMC-FDU-TZBC-NO_2 co-incubated with NTR. A IMC-FDU-TZBC-NO_2 solution (100 μM) was prepared by dissolving IMC-FDU-TZBC-NO_2 in PBS buffer (containing 0.1% DMSO, pH=7.4). Then, the IMC-FDU-TZBC-NO_2 solution and 10 μg/mL NTR solution (with 2 mM NADH) were stirred for different time (1, 2, 3, 4, 5, 6, 7, 8, 9, 10, 11, 12, 13, 11, 12, 13, 14, 15, 16, 17, and 18 min) at 37 ^{o}C under hypoxia conditions. Fluorescence measurements were performed in a 2.5 × 10 mm quartz cell on a luminescence spectrophotometer (λ_{ex}=380 nm, emission was collected at 400-700 nm).

Drug release. FDU solution (1 mM) was diluted by PBS buffer solution (pH=7.4) into 25, 50, 75, and 100 μM. The standard curve between concentration and peak area was detected through HPLC.

Then, 100 μM IMC-FDU-TZBC-NO_2 solution was mixed with 10 μg/mL NTR solution (with 2 mM NADH) and stirred at 37 °C under hypoxia conditions for different time (0, 1, 2, 3, 4, 5, 6, 7, 8, 9, 10, 11, 12, 13, 14, 15, 16, 17, and 18 min). Then, the FDU concentrations were detected through HPLC based on concentration-peak area standard curve.

The chemical composition of IMC-FDU-TZBC-NO_2 reacted with $Na_2S_2O_4$. $Na_2S_2O_4$ (40 mg, 0.23 mmol) and 100 mL of IMC-FDU-TZBC-NO_2 solution (200 μM) were stirred for 0.5 h. Then, the composition of the solution was detected by comparison of HPLC retention times of IMC-TZBCM, FDU, and IMC-FDU-TZBC-NO_2 (at 254 nm).

The analysis was performed using a gradient elution beginning with 5/95 (*V*/*V*) water (containing 0.1% TFA)/CAN, which was reaching 50/50 water (containing 0.1% TFA)/ACN within 7 min, and then to 60/40 water (containing 0.1% TFA)/ACN within 15-20 min, and finally to 100/0 water (containing 0.1% TFA)/ACN within 20-30 min. Flow ratewas 1 mL/min.

Selectivity of IMC-FDU-TZBC-NO_2. 10 mL of IMC-FDU-TZBC-NO_2 solution (200 μM) was mixed with 10 mL of 20 μg/mL NTR solution (with 2 mM NADH) and stirred for 24 h. Similarly, 10 mL of IMC-FDU-TZBC-NO_2 solution (200 μM) was mixed with 10 mL of 20 mM glutathione, cysteine, ascorbic acid, glutamate, fructose, aspartic acid, methionine, alanine, $CuCl_2$, KCl, $FeCl_3$, $FeCl_2$, $ZnCl_2$, Na_2SO_3, or Na_2S, respectively. All fluorescence measurements were performed on a fluorescence spectrophotometer (λ_{ex}=380 nm, collected from 400 to 700 nm, 5/5 nm slit width).

Stability of IMC-FDU-TZBC-NO_2 in blood serum. IMC-FDU-TZBC-NO_2 solution (1 mmol/L) was diluted into 200 μM with DMSO/PBS solution (pH=7.4, DMSO/PBS=1/999). Then, the IMC-FDU-TZBC-NO_2 solution (200 μM) was diluted into 100 μM with 10% of fetal bovine serum. Protected from light at 37 °C, the fluorescence intensity of IMC-FDU-TZBC-NO_2 solution was measured at 0, 4, 8, 12, 16, 20, and 24 h by fluorescence spectrophotometer ($\lambda_{ex/em}$=380/480 nm).

Influence of pH on stability of IMC-FDU-TZBC-NO_2. IMC-FDU-TZBC-NO_2 solution (1 mM) were diluted into 100 μM by PBS buffer solutions with different pH (2, 3, 4, 5, 6, 7, 8, 9, 10, 11, or 12) and stirred at 37°C for 0.5 h. The fluorescence intensity was determined.

Next, the IMC-FDU-TZBC-NO_2 solutions in different pH (2, 3, 4, 5, 6, 7, 8, 9, 10, 11, or 12) were mixed with 10 μg/mL NTR solution (with 2 mM NADH) and stirred at 37 °C under hypoxia conditions for 0.5 h. The fluorescence intensity was determined.

Cytotoxicity. HepG-2 or BRL-3A cells (2×10^4 cells/mL) seeded in 96 well plates were incubated in normal oxygen levels at 37 °C for 12 h. Subsequently, the cells were co-incubated with IMC-TZBCM, FDU, or IMC-FDU-TZBC-NO_2 solution (1, 5, 10, 15, or 20 μM) under hypoxia (1% O_2) or normoxia conditions for another 12 h, respectively. Then, the cells were incubated under normoxic conditions for 12 or 36 h. Subsequently, the cells were co-incubated with 20 mL of MTT (5 mg/mL) for another 4 h. At last, the supernatant was dissolved with 100 μL of DMSO, and the absorbance was determined at 570 nm by a microplate reader. Wells containing culture medium without cells were used as blanks.

The cultivation of tumor spheres. The HepG-2 spheres were cultured according to reported method.[60]

Confocal microscopy imaging. HepG-2 cells (2×10^4 cells/mL) seeded in 96 well plates were incubated in normal oxygen levels at 37 °C for 12 h. Subsequently, the cells and IMC-FDU-TZBC-NO_2 (10 μM) were co-incubated under normoxia or different hypoxia (10% O_2, 5% O_2, or 1% O_2) conditions at 37 °C for 12 h. Next, the cells were labeled with Lyso-Tracker Red (30

μg/mL) for 0.5 h and rinsed with PBS buffer twice to remove the medium. Fluorescence imaging was performed at λ_{ex}=405 nm.

The co-incubation and imaging of HepG-2 spheres with IMC-FDU-TZBC-NO_2 (10 μM) and Lyso-Tracker Red (30 μg/mL) were performed as the same method.

HepG-2 cells were pretreated in DMEM for 12 h, and washed with PBS buffer (×3). To test the inhibition effect of IMC, HepG-2 cells were incubated with IMC (500 μM) for 12 h and washed with PBS buffer (×3). Then, the HepG-2 cells were incubated with IMC-FDU-TZBC-NO_2 (10 μM) in fresh culture medium under different hypoxia (1% O_2 or 5% O_2) conditionsat 37 ^oC for 12 h. Next, the cells were labeled with Lyso-Tracker Red (30 μg/mL). After being treated 0.5 h, the cells were rinsed twice with PBS buffer to remove the medium. Fluorescence imaging was performed at λ_{ex}= 405 nm.

Cellular uptake. HepG-2 cells (1×10^5 cells per well) were seeded in 6-well plates for 24 h. Then, HepG-2 cells in a 6-well plate were divided into four groups. The first group, HepG-2 cells and FDU-TZBC-NO_2 (10 μM) were co-incubated for 12 h. The second group, HepG-2 cells and IMC-FDU-TZBC-NO_2 (10 μM) were co-incubated for 12 h. The third group, HepG-2 cells were pre-incubated with IMC (500 μM) for 12 h, and then were co-incubated with IMC-FDU-TZBC-NO_2 (10 μM) for another 12 h. The fourth group used as the control was treated with PBS. All four groups were cultured under the same conditions (1% O_2 or 5% O_2) at 37 ^oC. Single cell suspensions were serially prepared by trypsin digestion and washed with PBS. Afterwards, cells were analyzed by FACS-Calibur flow cytometer.

Hemolysis assessment. Fresh blood (2 mL) of BALB/c (nu/nu) mouse eyeballs was added 4 mL normal saline and centrifuged to discard the supernatant. The collected red blood cells was washed with normal saline until the supernatant was clear and suspended into normal saline solution assigned to 10%. 0.2 mL of red cell suspension was mixed with 0.8 mL IMC-FDU-TZBC-NO_2 with different concentrations (1, 5, 10, 15, and 20 mg/mL), 0.8 mL water as positive control and 0.8 mL normal saline as negative control. Each group was divided into 3 parallel groups, incubated at 37 ^oC for 30 min and the supernatant was obtained by çentrifugation. Samples were taken from 100 μL to 96 well plates, and the absorbance was measured at 545 nm.

***In vivo* antitumor activity.** Animal experiments were conducted according to the guidelines of the Hebei University Animal Welfare and Ethical Committee. Balb/c (nu/nu) mice (about 20 g, 4 weeks old) were fed in animal room (temperature: 20±2 ^oC; relative humidity: 60±10%; illumination time: 12 h) with free access to water and food. HepG-2 cells (around 1×10^7 cells each mouse) were injected into the right flank of the nude mice, all of which developed tumors in 7 d with sizes of about 50 mm^3 by average. These mice were assigned into 3 groups (5 mice/group) randomly, and treated by IMC-FDU-TZBC-NO_2, FDU-TZBC-NO_2 and PBS (control group) *via* tail vein injection (10 mg/kg) every 3 d, respectively. Tumor volume was recorded. All mice were sacrificed 22 d after the first treatment, the tumors and major organs (heart, liver, spleen, lung, and kidney) were excised, weighed and fixed with formalin for paraffin embedding.

Histological examination of tumor tissues. The excised tumors (or Heart, liver, spleen, lung, and kidney) were fixed using 4% formalin, embedded in paraffin and sectioned into 5 um thick slices. The sections were stained with H&E for histological examinations and observed under inverted microscope.

Notes

The authors declare no competing financial interests.

■ ACKNOWLEDGMENTS

This work was supported by the Priority Strategy project of Key Laboratory of Medicinal Chemistry and Molecular Diagnosis of Ministry of Education (No. ts2019001), the Natural Science Foundation of Hebei Province (No. B2019201444, B2019201333), and the Postgraduate's Innovation Fund Project of Hebei University (hbu2019ss008).

■ REFERENCES

(1) Chen, W., Zheng, R., Zhang, S., Zeng, H., Zuo, T., Xia, C., Yang, Z., and Jie, H. (2017) Cancer incidence and mortality in China in 2013: an analysis based on urbanization level. *Chinese J. Cancer Res*. *29*, 1–10.

(2) Guo. Y., Zhang. P., Zhao, Q., Wang, K., and Luan, Y. (2016) Reduction-sensitive polymeric micelles based on docetaxel-polymer conjugates via disulfide linker for efficient cancer therapy. *Macromol. Biosci. 16,* 420–431.

(3) Philpot, R.M. (2015) Potential use of nicotinic receptor agonists for the treatment of chemotherapy-induced cognitive deficits. *Neurochem. Res. 40*, 2018–2031.

(4) Gottesman, M.M., Fojo, T., and Bates, S.E. (2002) Multidrug resistance in cancer: role of ATP–dependent transporters. *Nat. Rev. Cancer 2*, 48–58.

(5) Kumar, R., Han, J., Lim, H.J., Ren, W.X., Lim, J.Y., Kim, J.H., and Kim, J.S. (2014) Mitochondrial induced and self-monitored intrinsic apoptosis by antitumor theranostic prodrug: in vivo imaging and precise cancer treatment. *J. Am. Chem. Soc. 136*, 17836–17843.

(6) Lee, M.H., Kim, E.J., Lee, H., Kim, H.M., Chang, M.J., Park, S.Y., Hong, K.S., Kim, J.S., and Sessler, J.L. (2016) Liposomal texaphyrin theranostics for metastatic liver cancer. *J. Am. Chem. Soc. 138*, 16380–16387.

(7) Yuan, Y., and Liu, B. (2017) Visualization of drug delivery processes using AIEgens. *Chem. Sci. 8*, 2537–2546.

(8) Novohradsky, V., Zamora, A., Gandioso, A., Brabec, V., Ruiz, J., and Marchan, V. (2017) Somatostatin receptor-targeted organometallic iridium(III) complexes as novel theranostic agents. *Chem. Commun. 53*, 5523–5526.

(9) Du, J., Du, X., Mao, C.Q., and Wang, J. (2011) Tailor-made dual pH-sensitive polymer-doxorubicin nanoparticles for efficient anticancer drug delivery, *J. Am. Chem. Soc. 133*, 17560–17563.

(10) Li, S., Hu, K., Cao, W., Sun, Y., Sheng, W., Li, F., Wu, Y., and Liang, X.J. (2014) pH-responsive biocompatible fluorescent polymer nanoparticles based on phenylboronic acid for intracellular imaging and drug delivery. *Nanoscale 6*, 13701–13709.

(11) Wang, Y., Du, J., Wang, Y., Jin, Q., and Ji, J. (2015) Pillar[5]arene based supramolecular prodrug micelles with pH induced aggregate behavior for intracellular drug delivery, *Chem. Commun.* 51, 2999–3002.

(12) Wang, H., Liu, G., Dong, S., Xiong, J., Du, Z., and Cheng, X. (2015) A pH-responsive AIE nanoprobe as a drug delivery system for bioimaging and cancer therapy. *J. Mater. Chem. B 3*, 7401–7407.

(13) Zhang, N., Su, Z., Liang, Y., Yao, Y., and Wang, T. (2016) Polymeric complex micelles based on double-hydrazone linkage and dual drug-loading strategy for pH-sensitive docetaxel delivery. *J. Mater. Chem. B 4,* 1122–1133.

(14) Zhong, Y., Goltsche, K., Cheng, L., Xie, F., Meng, F., Deng, C., Zhong, Z., and Haag, R. (2016)

Hyaluronic acid-shelled acid-activatable paclitaxel prodrug micelles effectively target and treat CD44-overexpressing human breast tumor xenografts *in vivo*. *Biomaterials 84*, 250–261.

(15) Silvers, W.C., Prasai, B., Burk, D.H., Brown, M.L., and Mccarley, R.L. (2013) Profluorogenic reductase substrate for rapid, selective, and sensitive visualization and detection of human cancer cells that overexpress NQO1. *J. Am. Chem. Soc. 135*, 309–314.

(16) Ueki, N., Lee, S., Sampson, N.S., Hayman, and M.J. (2013) Selective cancer targeting with prodrugs activated by histone deacetylases and a tumour-associated protease. *Nat. Commun. 4*, 2735.

(17) Hettiarachchi, S.U., Prasai, B., and Mccarley, R.L. (2014) Detection and cellular imaging of human cancer enzyme using a turn-on, wavelength-shiftable, self-immolative profluorophore. *J. Am. Chem. Soc. 136*, 7575–7578.

(18) Callmann, C.E., Barback, C.V., Thompson, M.P., Hall, D.J., Mattrey, R.F., and Gianneschi, N.C. (2015) Therapeutic enzyme-responsive nanoparticles for targeted delivery and accumulation in tumors. *Adv. Mater. 27*, 4611–4615.

(19) Adams. B.T., Nicoli, S., Chowdhury, M.A., Esank, A.N.K., Lees, S.J., Rempel, B.P., and Phenix, C.P. (2015) *N*-Alkylated aziridines are easily-prepared, potent, specific and cell-permeable covalent inhibitors of human β-glucocerebrosidase. *Chem. Commun*. *51*, 11390–11393.

(20) Tang, Y., Wu, Z., Zhang, C.H., Zhang, X.L., and Jiang, J.H. (2016) Enzymatic activatable self-assembled peptide nanowire for targeted therapy and fluorescence imaging of tumors. *Chem. Commun. 52*, 3631–3634.

(21) Jang, J.H., Lee, H., Sharma, A., Lee, S.M., Lee, T.H., Kang, C., and Kim, J.S. (2016) Indomethacin-guided cancer selective prodrug conjugate activated by histone deacetylase and tumour-associated protease. *Chem. Commun. 52*, 9965–9968.

(22) Hagen, H., Marzenell, P., Jentzsch, E., Wenz, F., Veldwijk, M.R., and Mokhir, A. (2012) Aminoferrocene-based prodrugs activated by reactive oxygen species. *J. Med. Chem.* 55, 924–934.

(23) Zhang, H., Zhu, X., Ji, Y., Jiao, X., Chen, Q., Hou, L., Zhang, H., and Zhang, Z. (2015) Near-infrared-triggered in-situ hybrid hydrogel system for synergistic cancer therapy. *J. Mater. Chem. B 3*, 6310–6326.

(24) Perez, C., Monserrat, J.P., Chen, Y., and Cohen, S.M. (2015) Exploring hydrogen peroxide responsive thiazolidinone-based prodrugs. *Chem. Commun. 51*, 7116–7119.

(25) Deng, H., Zhao, X., Liu, J., Deng, L., Zhang, J., Liu, J., and Dong, A. (2015) Reactive oxygen species (ROS) responsive PEG–PCL nanoparticles with pH-controlled negative-to-positive charge reversal for intracellular delivery of doxorubicin. *J. Mater. Chem. B 3*, 9397–9408.

(26) Li, Q., Wen, Y., You, X., Zhang, F., Shah, V., Chen, X., Tong, D., Wei, X., Yin, L., and Wu, J. (2016) Development of a reactive oxygen species (ROS)-responsive nanoplatform for targeted oral cancer therapy, *J. Mater. Chem. B 4,* 4675–4682.

(27) Liu, X., Xiang, J., Zhu, D., Jiang, L., Zhou, Z., Tang, J., Liu, X., Huang, Y., and Shen, Y. (2016) Gene delivery: fusogenic reactive oxygen species triggered charge-reversal vector for effective gene delivery. *Adv. Mater. 28*, 1714–1714.

(28) Li, B., Liu, P., Yan, D., Zeng, F., and Wu, S. (2017) A self-immolative and DT-diaphorase-activatable prodrug for drug-release tracking and therapy. *J. Mater. Chem. B 5*, 2635–3643.

(29) Furgeson, D.Y., Dreher, M.R., and Chilkoti, A. (2006) Structural optimization of a "smart" doxorubicin–polypeptide conjugate for thermally targeted delivery to solid tumors. *J. Control. Release* 110, 362–369.

(30) Ha, W., Yu, J., Song, X.Y., Chen, J., and Shi, Y.P. (2014) Tunable temperature-responsive

supramolecular hydrogels formed by prodrugs as a codelivery system. *ACS Appl. Mater. Inter. 6*, 10623–10630.

(31) Lin, Q., Huang, Q., Li, C., Bao, C., Liu, Z., Li, F., and Zhu, L. (2010) Anticancer drug release from a mesoporous silica based nanophotocage regulated by either a one- or two-photon process. *J. Am. Chem. Soc. 132,* 10645–10647.

(32) Dcona, M.M., Mitra, D., Goehe, R.W., Gewirtz, D.A., Lebman, D.A., and Hartman, M.C.T. (2012) Photocaged permeability: a new strategy for controlled drug release. *Chem. Commun*. *48*, 4755–4757.

(33) Han, K., Zhu, J.Y., Wang, S.B., Li, Z.H., Cheng, S.X., and Zhang, X.Z. (2015) Tumor targeted gold nanoparticles for FRET-based tumor imaging and light responsive on-demand drug release. *J. Mater. Chem. B 3*, 8065–8069.

(34) Brahimi-Horn, M.C., Chiche, J., and Pouyssegur, J. (2007) Hypoxia and cancer. *J. Mol. Med. 85*, 1301–1307.

(35) Bristow, R.G., and Hill, R.P. Hypoxia and metabolism. (2008) Hypoxia, DNA repair and genetic instability. *Nat. Rev. Cancer 8*, 180–192.

(36) Liao, D., and Johnson, R.S. (2007) Hypoxia: a key regulator of angiogenesis in cancer. *Cancer Metast. Rev. 26*, 281–290.

(37) Vaupel, P. (2008) Hypoxia and aggressive tumor phenotype: implications for therapy and prognosis. *Oncologist 13,* 21–26.

(38) Chang, Q., Jurisica, I., Do, T., and Hedley, D.W. (2011) Hypoxia predicts aggressive growth and spontaneous metastasis formation from orthotopically grown primary xenografts of human pancreatic cancer. *Cancer Res. 71*, 3110–3120.

(39) Brown, J.M., and Wilson, W.R. (2004) Exploiting tumour hypoxia in cancer treatment, *Nat. Rev. Cancer,* 4, 437–447.

(40) Liu, J., Liu, Y., Bu, W., Bu, J., Sun, Y., Du, J., and Shi, J. (2014) Ultrasensitive nanosensors based on upconversion nanoparticles for selective hypoxia imaging in vivo upon near-infrared excitation. *J. Am. Chem. Soc. 136*, 9701–9709.

(41) Zheng, X., Wang, X., Mao, H., Wu, W., Liu, B., and Jiang, X. (2015) Hypoxia-specific ultrasensitive detection of tumours and cancer cells *in vivo*. *Nat. Commun. 6,* 5834.

(42) Feng, W., Gao, C., Liu, W., Ren, H., Wang, C., Ge, K., Li, S., Zhou, G., Li, H., Wang, S., and et al. (2016) A novel anticancer theranostic pro-prodrug based on hypoxia and photo sequential control. *Chem. Commun. 52*, 9434–9437.

(43) Liu, J., Bu, W., and Shi, J. (2017) Probes for imaging and treating tumor hypoxia. *Chem. Rev. 117*, 6160–6224.

(44) Kling, J. (2012) Hypoxia-activated prodrugs forge ahead in cancer. *Nat. Biotechnol*. *30*(5), 381.

(45) Hunter, F.W., Wouters, B.G., and Wilson, W.R. (2016) Hypoxia-activated prodrugs: paths forward in the era of personalised medicine. *Br. J. Cancer 114*, 1071–1077.

(46) Sellers, R.S., Radi, Z.A., and Khan, N.K. (2010) Pathophysiology of cyclooxygenases in cardiovascular homeostasis, *Vet. Pathol. 47*, 601–613.

(47) Nath, S., Roy, L.D., Grover, P., Rao, S., and Mukherjee, P. (2015) Mucin 1 regulates Cox-2 gene in pancreatic cancer. *Pancreas, 44*, 909–917.

(48) Wang, D., and Dubois, R.N. (2010) The role of COX-2 in intestinal inflammation and colorectal cancer. *Oncogene 29,* 781–788.

(49) Subbaramaiah, K., and Dannenberg, A.J. (2003) Cyclooxygenase 2: a molecular target for cancer prevention and treatment. *Trends Pharmacol. Sci. 24*, 96–102.

(50) Echizen, K., Hirose, O., Maeda, Y., and Oshima, M. (2016) Inflammation in gastric cancer: Interplay of the COX-2/prostaglandin E2 and Toll-like receptor/MyD88 pathways. *Cancer Sci. 107*, 391–397.

(51) Rizzo, M. T. (2011) Cyclooxygenase-2 in oncogenesis. *Clin. Chim. Acta. 412*, 671–687.

(52) Hua, Z., Fan, J., Wang, J., Dou, B., Fan, Z., Cao, J., Qu, J., Zhi, C., Zhao, W., and Peng, X. (2014) Fluorescence discrimination of cancer from inflammation by molecular response to COX-2 enzymes. *J. Am. Chem. Soc. 135*, 17469–17475.

(53) Uddin, M.J., Crews, B.C., Ghebreselasie, K., and Marnett, L.J. (2013) Design, synthesis, and structure–activity relationship studies of fluorescent inhibitors of cycloxygenase-2 as targeted optical imaging agents, *Bioconjugate Chem. 24*, 712–723.

(54) Flower, R.J. (2003) The development of COX2 inhibitors. *Nat. Rev. Drug Discov.* 2, 179–191.

(55) Nakagawa, H., Maeda, N., Tsuzuki, T., Suzuki, T., Hirayama, A., Miyahara, E., and Wada, K. (2001) Intracavitary chemotherapy with 5-fluoro-2'-deoxyuridine (FdUrd) in malignant brain tumors. *Jpn. J. Clin. Oncol. 31,* 251–258.

(56) Tsume, Y., Hilfinger, J.M., and Amidon, G.L. (2008) Enhanced cancer cell growth inhibition by dipeptide prodrugs of floxuridine: increased transporter affinity and metabolic stability. *Mol. Pharm. 5*, 717–727.

(57) Dannenberg, A.J., Lippman, S.M., Mann, J.R., Subbaramaiah, K., and DuBois, R.N. (2005) Cyclooxygenase-2 and epidermal growth factor receptor: pharmacologic targets for chemoprevention. *J. Clin. Oncol. 23*, 254–266.

(58) Feng, W., Wang Y.,, Chen, S., Wang, C., Wang, S., Li, S., Li, H., Zhou, G., and Zhang, J. (2016) 4-Nitroimidazole-3-hydroxyflavone conjugate as a fluorescent probe for hypoxic cells. *Dyes Pigments 131*, 145–153.

(59) Li, H., Lei, W., Wu, J., Li, S., Zhou, G., Liu, D., Yang, X., Wang, S., Li, Z., and Zhang, J. (2018) An upconverting nanotheranostic agent activated by hypoxia combined with NIR irradiation for selective hypoxia imaging and tumour therapy. *J. Mater. Chem. B 6*, 2747–2757.

(60) Liu, W., Liu, H., Peng, X., Zhou, G., Liu, D., Li, S., Zhang, J., and Wang, S. (2018) Hypoxia-activated anticancer prodrug for bioimaging, tracking drug release, and anticancer application, *Bioconjugate Chem. 29*, 3332–3343.

(61) Sun, Q., Ojha, T., Kiessling, F., Lammers, T., and Shi, Y. (2017) Enhancing tumor penetration of nanomedicines. *Biomacromolecules 18*, 1449–1459.

(62) Wang, W., Bundgaard, H., Buur, A., and Lee, V.H. (1991) Corneal penetration of 5-fluorouracil and its improvement by prodrug derivatization in the albino rabbit: implication in glaucoma filtration surgery. *Curr. Eye Res. 10*, 87–97.

Scheme 1.

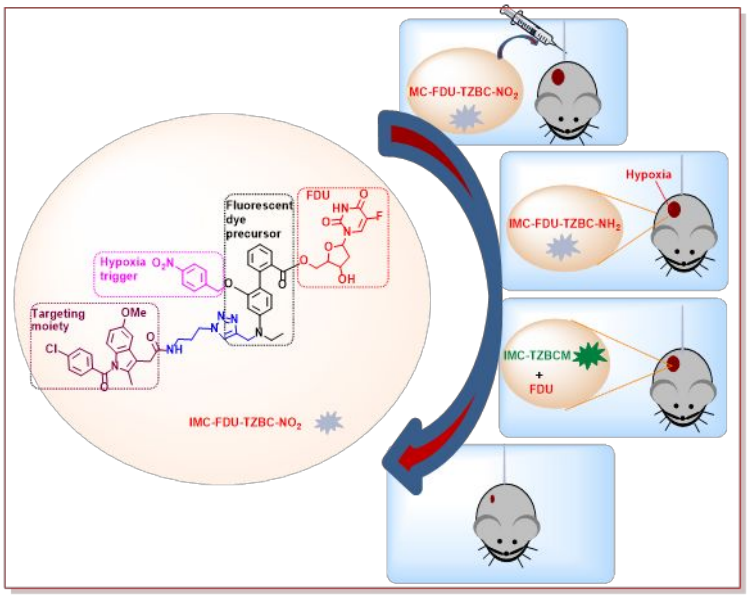
MC-FDU-TZBC-NO2
Hypoxia
IMC-FDU-TZBC-NH2
IMC-TZBCM
+
FDU
Fluorescent dye precursor
FDU
Hypoxia trigger
Targeting moiety
IMC-FDU-TZBC-NO2

Scheme 2.

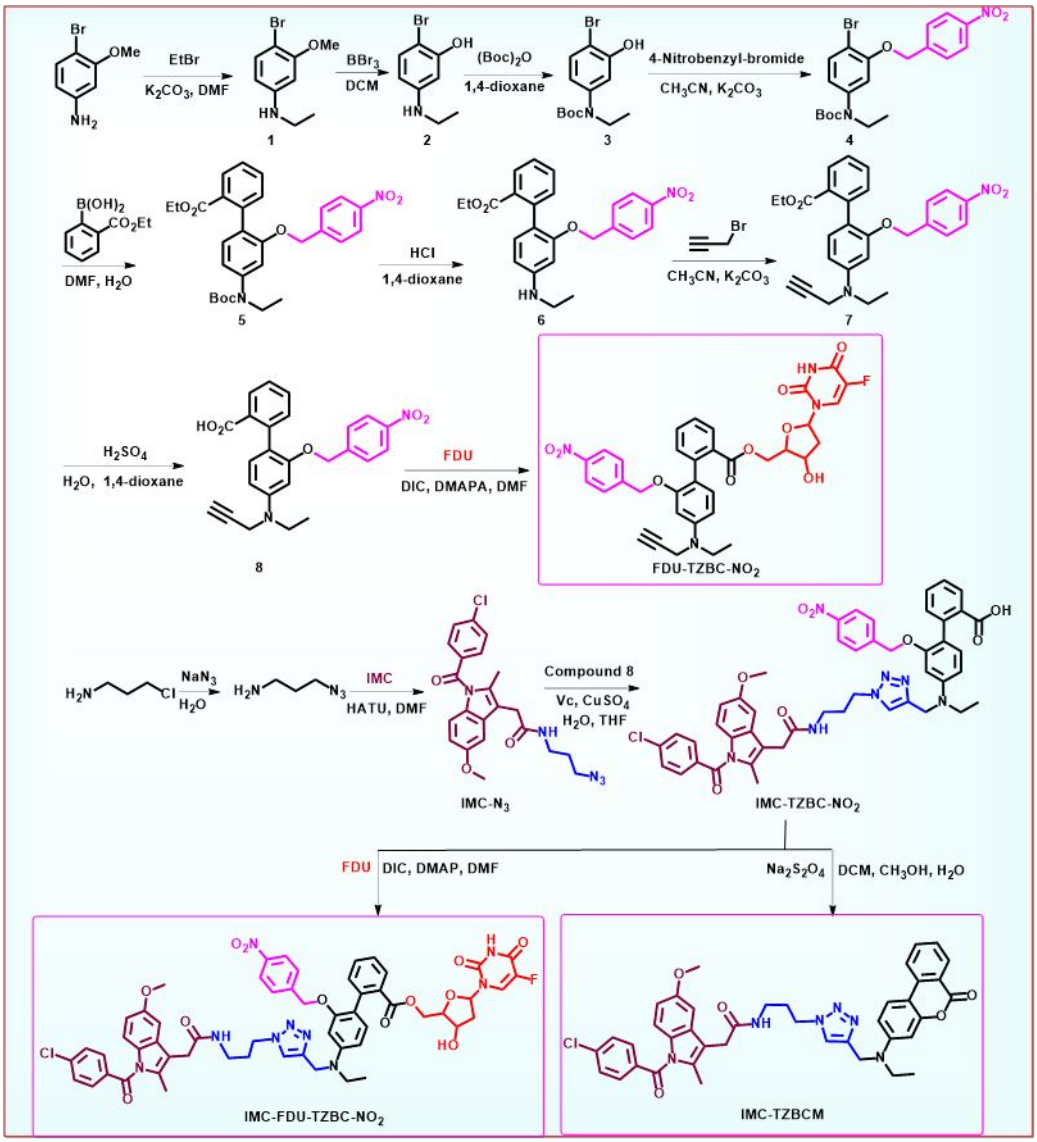
EtBr
K2CO3, DMF
BBr3
DCM
(Boc)2O
1,4-dioxane
4-Nitrobenzyl-bromide
CH3CN, K2CO3
1
2
3
4
DMF, H2O
HCl
1,4-dioxane
CH3CN, K2CO3
5
6
7
H2SO4
H2O, 1,4-dioxane
FDU
DIC, DMAPA, DMF
8
FDU-TZBC-NO2
NaN3
H2O
IMC
HATU, DMF
Compound 8
Vc, CuSO4
H2O, THF
IMC-N3
IMC-TZBC-NO2
FDU
DIC, DMAP, DMF
Na2S2O4
DCM, CH3OH, H2O
IMC-FDU-TZBC-NO2
IMC-TZBCM

Figure 1.

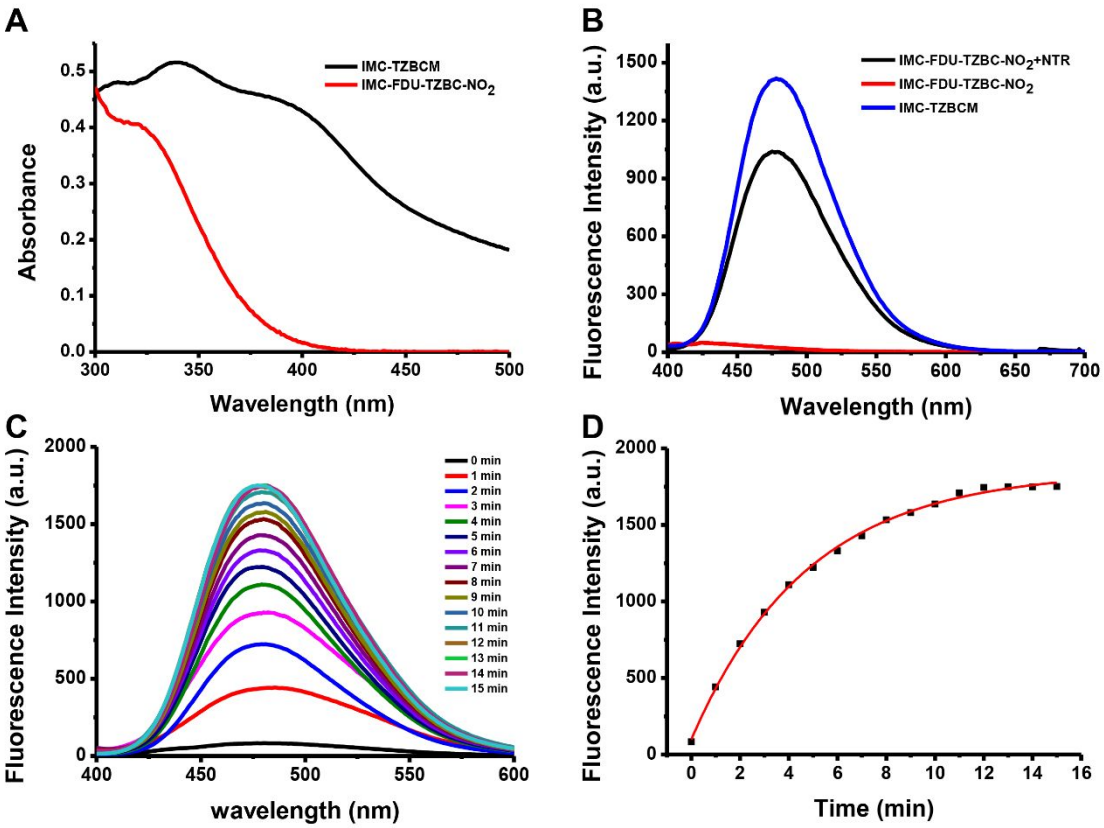

Figure 2

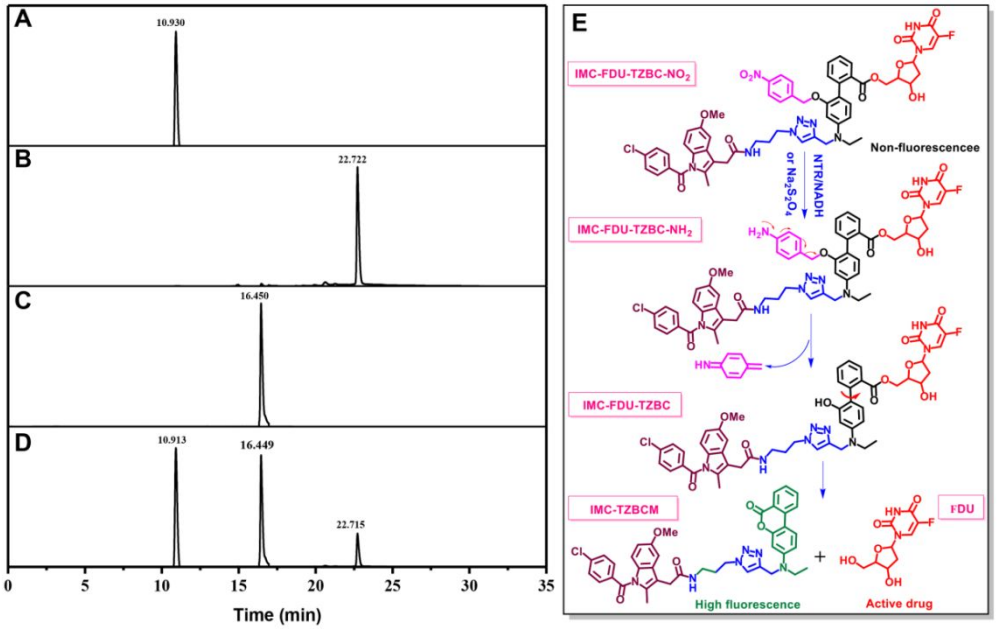
A
10.930
B
22.722
C
16.450
D
10.913
16.449
22.715
0 5 10 15 20 25 30 35
Time (min)
E
IMC-FDU-TZBC-NO2
Non-fluorescencee
or Na2S2O4
NTR/NADH
IMC-FDU-TZBC-NH2
IMC-FDU-TZBC
IMC-TZBCM
FDU
High fluorescence
Active drug

Figure 3

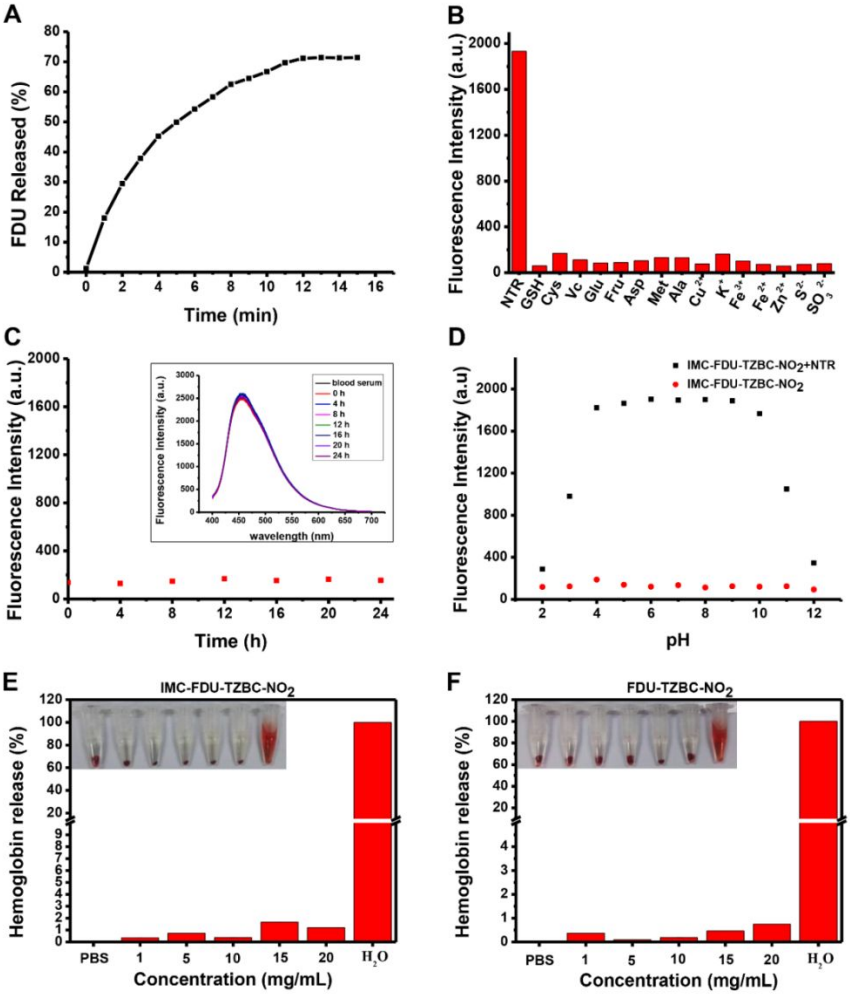
A
FDU Released (%)
Time (min)
B
Fluorescence Intensity (a.u.)
NTR GSH Cys Vc Glu Fru Asp Met Ala Cu2+ K+ Fe3+ Fe2+ Zn2+ S2- SO3 2-
C
Fluorescence Intensity (a.u.)
blood serum
0 h
4 h
8 h
12 h
16 h
20 h
24 h
wavelength (nm)
Time (h)
D
IMC-FDU-TZBC-NO2+NTR
IMC-FDU-TZBC-NO2
Fluorescence Intensity (a.u.)
pH
E
IMC-FDU-TZBC-NO2
Hemoglobin release (%)
PBS 1 5 10 15 20 H2O
Concentration (mg/mL)
F
FDU-TZBC-NO2
Hemoglobin release (%)
PBS 1 5 10 15 20 H2O
Concentration (mg/mL)

Figure 4

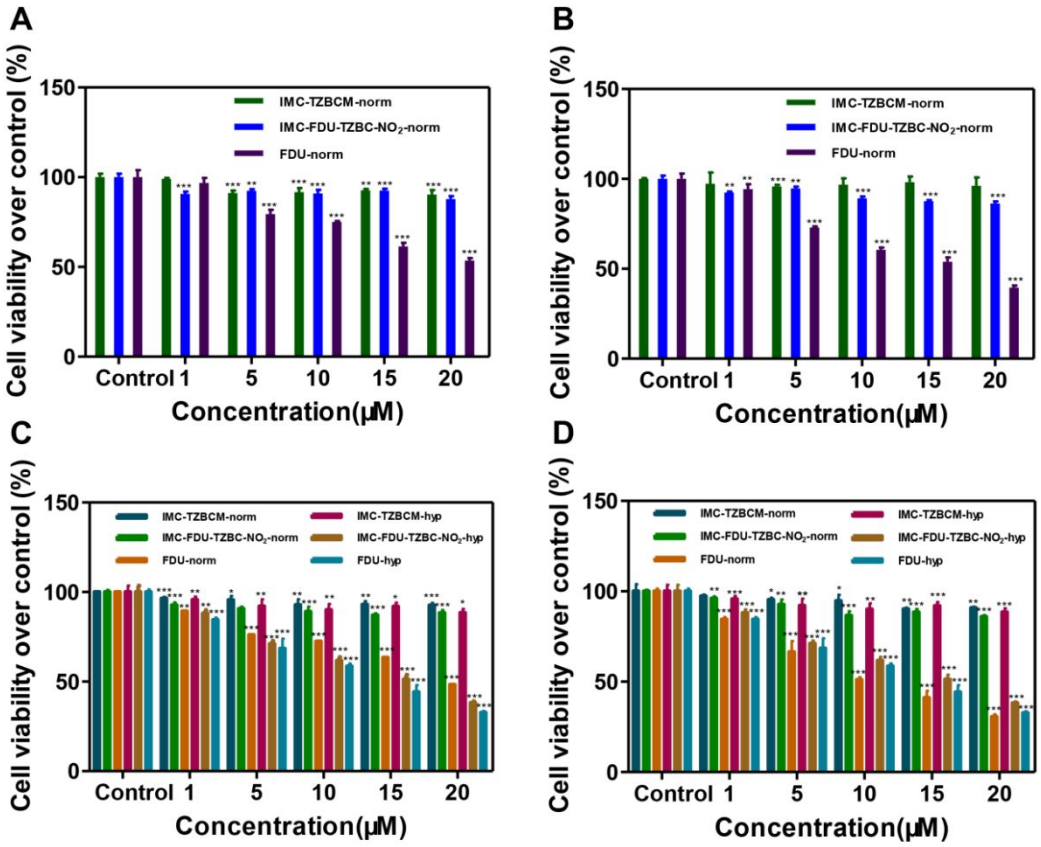
A
B
C
D
Cell viability over control (%)
Concentration(μM)
Control 1 5 10 15 20
0 50 100 150
IMC-TZBCM-norm
IMC-FDU-TZBC-NO2-norm
FDU-norm
IMC-TZBCM-hyp
IMC-FDU-TZBC-NO2-hyp
FDU-hyp

Figure 5

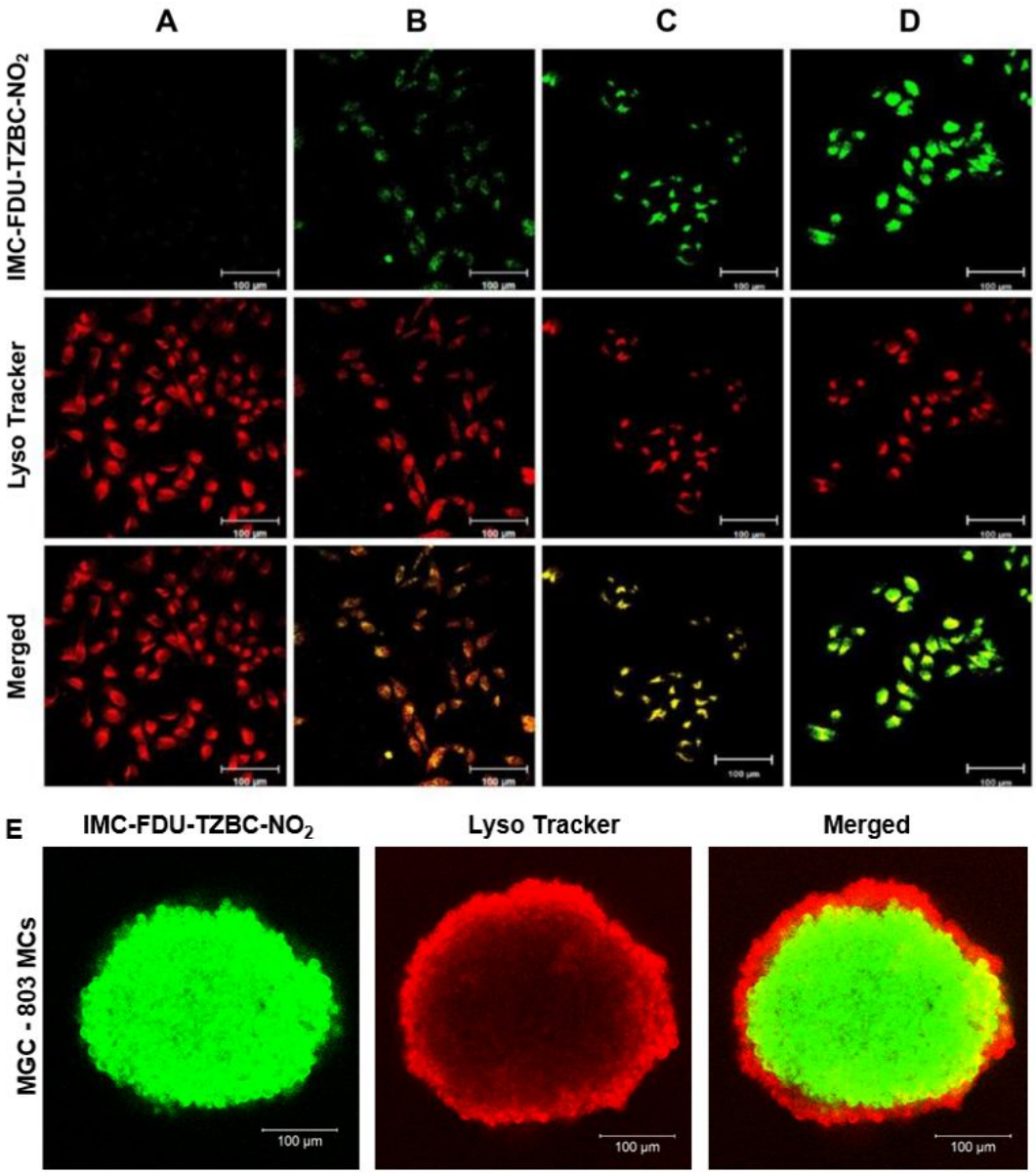
A
B
C
D
IMC-FDU-TZBC-NO2
Lyso Tracker
Merged
E
IMC-FDU-TZBC-NO2
Lyso Tracker
Merged
MGC - 803 MCs
100 μm
100 μm
100 μm

Figure 6

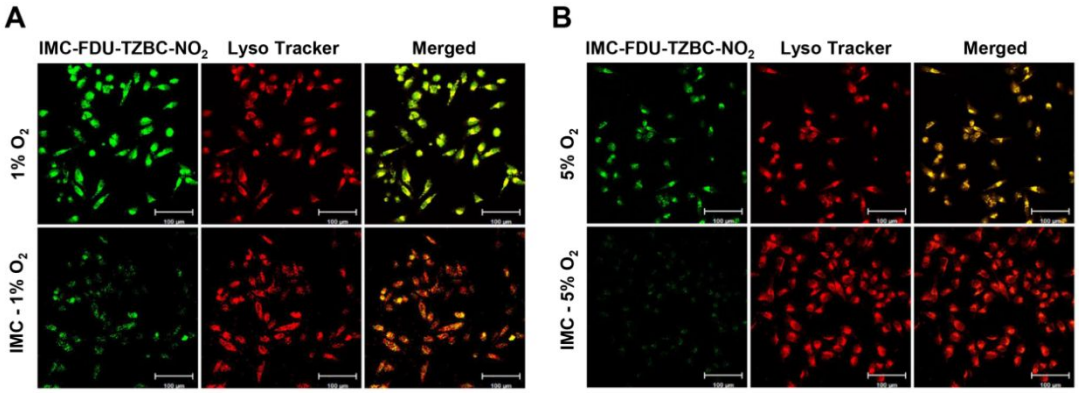
A
IMC-FDU-TZBC-NO2
Lyso Tracker
Merged
1% O2
IMC - 1% O2
B
IMC-FDU-TZBC-NO2
Lyso Tracker
Merged
5% O2
IMC - 5% O2

Figure 7

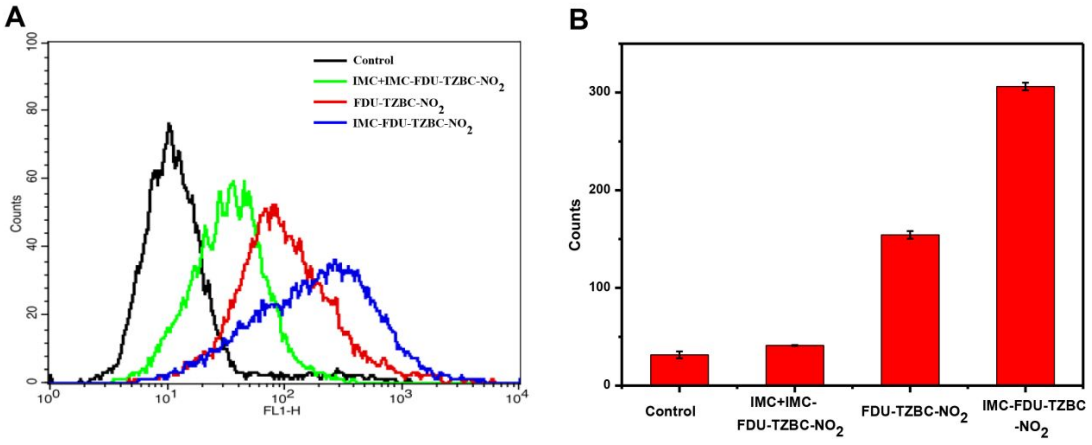

Figure 8

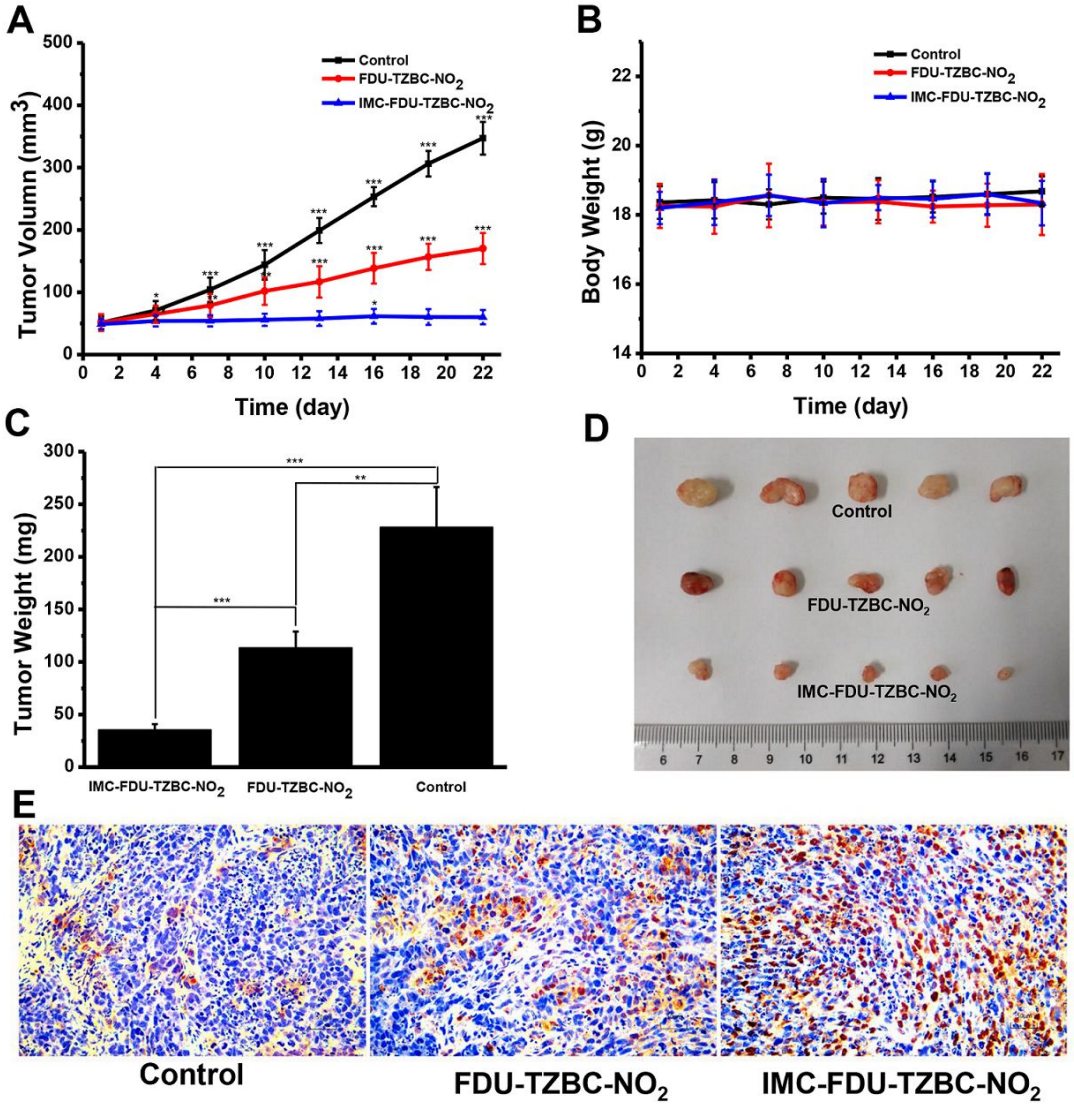

Figure 9

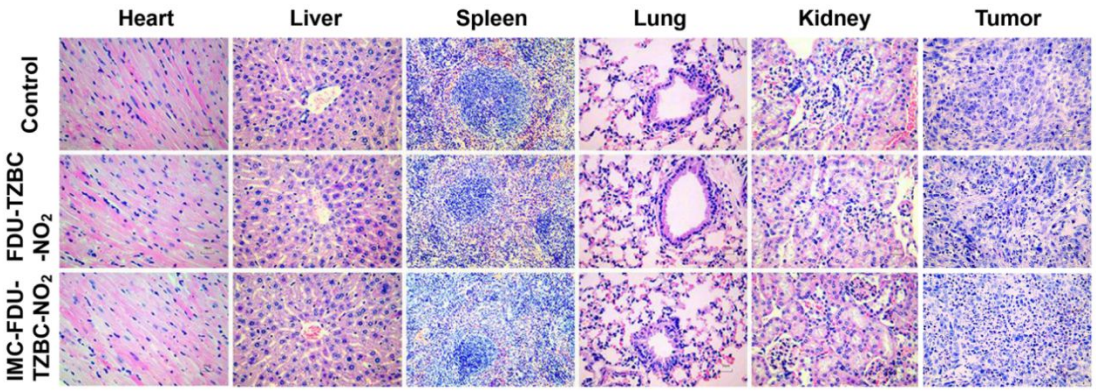
Heart
Liver
Spleen
Lung
Kidney
Tumor
Control
FDU-TZBC -NO2
IMC-FDU-TZBC-NO2